Role of precipitation uncertainty in the estimation of hydrologic soil properties using remotely sensed soil moisture in a semiarid environment

Christa D. Peters-Lidard,[1] David M. Mocko,[1,2,3] Matthew Garcia,[1,4] Joseph A. Santanello Jr.,[1,5] Michael A. Tischler,[6] M. Susan Moran,[7] and Yihua Wu[1,4,8]

Received 12 January 2007; revised 12 November 2007; accepted 7 December 2007; published 30 May 2008.

[1] The focus of this study is on the role of precipitation uncertainty in the estimation of soil texture and soil hydraulic properties for application to land-atmosphere modeling systems. This work extends a recent study by Santanello et al. (2007) in which it was shown that soil texture and related physical parameters may be estimated using a combination of multitemporal microwave remote sensing, land surface modeling, and parameter estimation methods. As in the previous study, the NASA-GSFC Land Information System modeling framework, including the community Noah land surface model constrained with pedotransfer functions (PTF) for use with the Parameter Estimation Tool, is applied to several sites in the Walnut Gulch Experimental Watershed (WGEW) in southeastern Arizona during the Monsoon '90 experiment period. It is demonstrated that the application of PTF constraints in the estimation process for hydraulic parameters provides accuracy similar to direct hydrologic parameter estimation, with the additional benefit of simultaneously estimated soil texture. Precipitation uncertainty is then represented with systematically varying sources, from the high-density precipitation gauge network in WGEW to lower quality sources, including spatially averaged precipitation, single gauges in and near the watershed, and results from the continental-scale North American Regional Reanalysis data set. It is demonstrated that the quality of the input precipitation data set, and particularly the accuracy of the data set, in both detection of convective (heavy) rainfall events and reproduction of the observed rainfall rate probabilities, is a critical determinant in the use of successive remote sensing results in order to establish and refine estimates of soil texture and hydraulic properties.

Citation: Peters-Lidard, C. D., D. M. Mocko, M. Garcia, J. A. Santanello Jr., M. A. Tischler, M. S. Moran, and Y. Wu (2008), Role of precipitation uncertainty in the estimation of hydrologic soil properties using remotely sensed soil moisture in a semiarid environment, *Water Resour. Res.*, *44*, W05S18, doi:10.1029/2007WR005884.

1. Introduction

[2] The simulation of soil moisture dynamics using land surface models (LSMs) has been addressed in a wide variety of studies and with models of various complexity [e.g., *Shao and Henderson-Sellers*, 1996; *Albertson and Montaldo*, 2003]. Soil moisture plays a well-known role in the energy and water budgets for land-atmosphere exchange [e.g., *Betts*, 2000; *Berbery et al.*, 2003; *Betts et al.*, 2003; *Findell and Eltahir*, 2003; *Koster et al.*, 2004]. As a result, important applications such as agriculture, water resource management, flood forecasts, and weather and climate prediction depend on our ability to predict soil moisture.

[3] However, soil moisture profiles required for these applications are not collected in situ on a routine basis except in sparse networks, such as that in Illinois [*Hollinger and Isard*, 1994] or throughout the USDA Soil Climate Analysis Network (SCAN) [*Schaefer and Paetzold*, 2001]. Archives of these and other historical soil moisture data sets are available at the Global Soil Moisture Data Bank [*Robock et al.*, 2000]. Soil moisture profiles are also collected and studied at experimental watersheds established by the USDA Agricultural Research Service (ARS), such as that managed by the Southwest Watershed Research Center at the Walnut Gulch Experimental Watershed (WGEW) [*Hymer et al.*, 2000] in southeastern Arizona. Other than these networks, soil moisture observations in particular locations are generally carried out during short-

[1]NASA Goddard Space Flight Center, Hydrological Sciences Branch, Greenbelt, Maryland, USA.
[2]NASA Goddard Space Flight Center, Climate and Radiation Branch, Greenbelt, Maryland, USA.
[3]Science Applications International Corporation, Beltsville, Maryland, USA.
[4]Goddard Earth Science and Technology Center, University of Maryland Baltimore County, Baltimore, Maryland, USA.
[5]Earth System Science Interdisciplinary Center, University of Maryland, College Park, Maryland, USA.
[6]Topographic Engineering Center, Engineer Research and Development Center, U.S. Army Corps of Engineers, Alexandria, Virginia, USA.
[7]Southwest Watershed Research Center, USDA Agricultural Research Service, Tuscon, Arizona, USA.
[8]Now at Science Applications International Corporation, NOAA National Weather Service, National Centers for Environmental Prediction, Camp Springs, Maryland, USA.

0043-1397/08/2007WR005884$09.00

term field experiments, many of which have highlighted the heterogeneous nature of soils by measurement of water content and texture [*Mohanty et al.*, 2002].

[4] Indirect, integrated estimates of soil moisture can be obtained using thermal infrared measurements [e.g., *Carlson et al.*, 1995]. However, other studies [e.g., *Entekhabi et al.*, 1994; *Houser et al.*, 1998] have suggested that the most promising approach to surface soil moisture estimation over time and space may be a combination of remote sensing and modeling. In general, microwave remote sensing methods using passive (radiometer) and active (radar) sensors have had the greatest success producing surface soil moisture estimates suitable for assimilation in LSMs [*Hollenbeck et al.*, 1996; *Moran et al.*, 2004; *Thoma et al.*, 2006]. Overall, none of the remote sensing methods provides an estimate of the vertical distribution of moisture in the soil column; the profile of soil moisture can, currently, only be estimated using modeling methods.

[5] In addition to the complexity and inherent nonlinearity of an LSM, the two primary uncertainties in soil moisture modeling are precipitation and soil hydraulic properties. Many soil models, including the community Noah LSM employed here, require the specification of hydraulic parameters in order to determine the vertical transport of moisture within the soil column by a simplified form of the one-dimensional *Richards'* [1931] equation. Hydraulic parameters are often derived from soil texture information, but the soil parameterization schemes often remain crude, inflexible, or inappropriate owing to the natural heterogeneity of the soils and a lack of detailed soil property maps. In some cases, the LSMs have been demonstrated to be more sensitive to the specification of soil hydraulic properties or soil textures than to the atmospheric forcing variables, including precipitation [*Gutmann and Small*, 2005; *Pitman*, 2003].

[6] In this work, the community Noah LSM [*Chen et al.*, 1996; *Ek et al.*, 2003] is applied to the simulation of soil moisture in the semiarid WGEW during the North American monsoon season. Water and energy balance predictions using the Noah LSM, in numerous versions, have been validated at the point scale [*Schlosser et al.*, 2000] and at watershed scales [*Bowling et al.*, 2003]. The Noah LSM is also one of several models incorporated into the NASA-GSFC Land Information System (LIS) [*Kumar et al.*, 2006], which provides a flexible software framework for the execution of LSMs with various methods for the specification of atmospheric forcing, surface conditions, and soil textures and hydraulic parameters.

[7] Because of their heritage in global and regional weather and climate modeling, all of the LSMs included in LIS contain simplifying assumptions with regard to their treatment of soil hydraulic and thermal properties. The LSMs also typically rely on texture-based lookup tables for the specification of these parameters. Recognizing the limitations in an approach based on discrete texture classes, numerous studies [e.g., *Gupta et al.*, 1999; *Hess*, 2001; *Liu et al.*, 2004; *Hogue et al.*, 2005] have attempted to optimize LSM parameters using observations such as soil moisture and surface temperature as constraints. While these studies highlight the potential for parameter estimation methods to derive large sets of "effective" parameters and to expose or diagnose specific model weaknesses, little progress has been made toward the determination of physically consistent parameter sets. Because of the complexity of estimation methods and the numbers of parameter sets employed in these studies, it has remained difficult to infer or derive any parameter information that could be applied to other, independent studies or models.

[8] With these issues in mind, *Santanello et al.* [2007] examined the potential for use of aircraft-based microwave radiometer and satellite-based radar retrievals of near-surface soil moisture with the Noah LSM to infer a physically consistent set of hydraulic parameters for the primary soil types found in the WGEW. One of the significant findings of *Santanello et al.* [2007] was that the success of this methodology was dependent on the number of remote sensing images acquired and the dynamic range in soil moisture captured by these images. It follows that the methodology should be similarly sensitive to the accuracy and range of precipitation data used as input to the LSM during the parameter estimation process. This work extends that study by examining the role of precipitation uncertainty in the parameter estimation process. This uncertainty is represented with a systematic variation of input precipitation from the high-density precipitation gauge network in WGEW to other, lower quality precipitation sources. We examine here the impacts of using precipitation gauges collocated with the soil moisture measurement sites, a single gauge located elsewhere within the WGEW, a first-order National Weather Service (NWS) synoptic site located approximately 100 km from the WGEW in Tucson, Arizona, and the continental-scale North American Regional Reanalysis (NARR) [*Mesinger et al.*, 2006] data set at one-third-degree spatial resolution over the region of interest.

[9] As in the study by *Santanello et al.* [2007], the LIS modeling framework and the Noah LSM are applied to selected sites in the WGEW during the Monsoon '90 field experiment. Constraints on the simulated evolution of soil moisture at the selected sites are provided by the application of pedotransfer functions (PTF) [e.g., *Cosby et al.*, 1984] and via calibration against in situ observations using the Parameter Estimation Tool (PEST) [*Doherty*, 2004]. In general, this work supports ongoing development of the Army Remote Moisture System (ARMS) [*Tischler et al.*, 2006] for the US Army Corps of Engineers. The supporting data sets for this study are described in section 2, including information on the experiment locations, soil moisture observations, and input precipitation data sets. The approach and methodology of these experiments are described further in section 3. Results of these experiments are described in section 4, and conclusions from this study are given in section 5.

2. Data

[10] The focus of this study is the Monsoon '90 field experiment carried out in the WGEW. Below, we briefly describe the watershed and the field experiment, as well as the unique soils and precipitation data that are the foundation for this work.

2.1. Walnut Gulch Experimental Watershed (WGEW)

[11] The WGEW, managed by the USDA ARS Southwest Watershed Research Center, is a 148 km^2 semiarid watershed in southeastern Arizona. The predominant soil

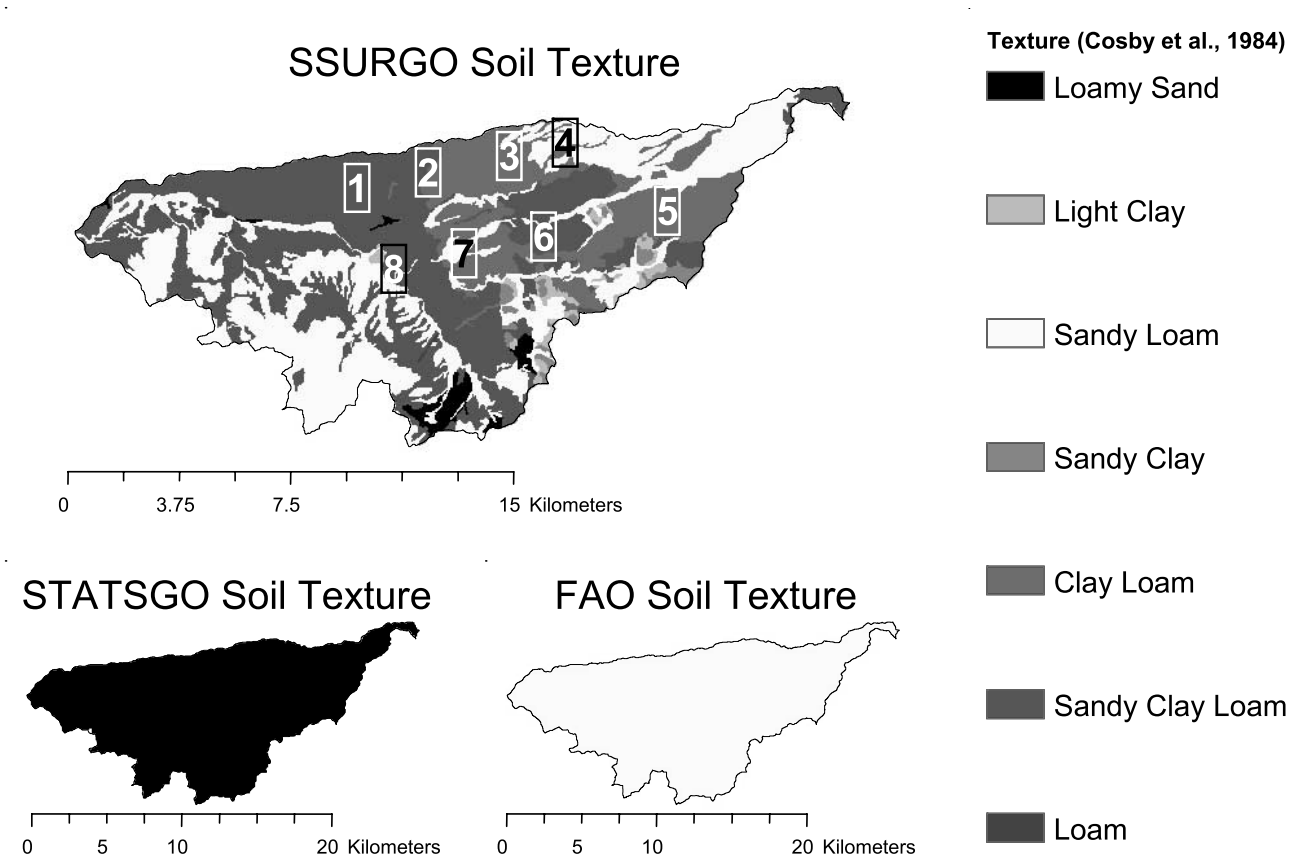

Figure 1. Soil texture classes in the Walnut Gulch Experimental Watershed (WGEW) from various data sets.

textures in the watershed are loamy sands and sandy loams, with a notable amount of coarse fragments. The vegetation throughout the watershed is generally a mixture of grasses and brush. The watershed is hilly with numerous channels, and contains more than 90 precipitation gauges and approximately 15 streamflow measurement stations.

2.2. Monsoon '90 Field Experiment

[12] The Monsoon '90 (hereafter M90) field experiment was conducted in the WGEW from June to September 1990 [*Kustas and Goodrich*, 1994]. During M90, intensive surface-based measurements were recorded at the eight "Metflux" sites indicated in Figure 1. These measurements included standard meteorological variables, surface fluxes of heat and moisture, and daily gravimetric soil moisture data. A NASA C-130 aircraft carried an airborne L-band Push Broom Microwave Radiometer (PBMR) from which surface soil moisture was derived from the measured microwave brightness temperature [*Schmugge et al.*, 1994]. The PBMR data was collected on 6 days during the height of the M90 experiment over the northern portion of the watershed, including the Metflux sites. Comparisons of the gravimetric soil moisture, measured to a depth of 5 cm, with the PBMR-derived observations during the M90 experiment demonstrated very good agreement, with a compound error of 4.5% ± 1.9%.

2.3. Soils Data

[13] For the application of an LSM to WGEW, there are several "standard" a priori sources of soil texture information. In order of increasing resolution, these include: the global United Nations Food and Agriculture Organization (FAO) Digital Soil Map of the World at a nominal resolution of 5 arc-min (∼8.5 km), which also contains derived information on some soil properties [*Food and Agriculture Organization*, 1996; *Reynolds et al.*, 1999; *Nachtergaele*, 2003]; the State Soil Geographic Database (STATSGO) data set [*Miller et al.*, 1994] at a nominal resolution of 15 arc-sec (∼400 m), including the "model-friendly" CONUS-SOIL multilayer soil characteristics data set [*Miller and White*, 1998]; and the county-level Soil Survey Geographic Database (SSURGO) [*U.S. Department of Agriculture, Natural Resources Conservation Service*, 2006] at a nominal resolution of approximately 1.5 arc-sec (∼40 m) in the region of the WGEW. The FAO, STATSGO and SSURGO soil texture maps for the WGEW are shown in Figure 1. Only one soil texture class is specified for the entire watershed in the FAO (sandy loam) and STATSGO (loamy sand) data sets, while the SSURGO data set specifies several classes in the WGEW including sandy loam and sandy clay loam. These soil types are referenced to the texture classes of *Cosby et al.* [1984] for the specification of hydraulic parameter values in the Noah LSM. The SSURGO data set also supplies maps of saturated hydraulic conductivity

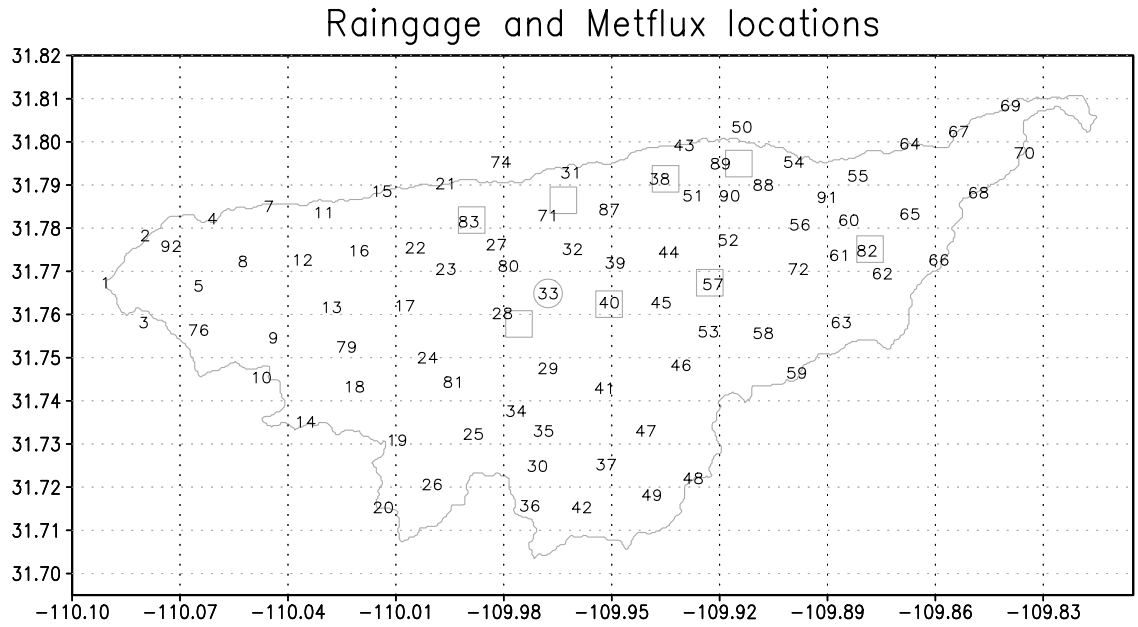

Figure 2. Precipitation gauge locations (numbered) and Monsoon '90 Metflux site locations (boxes) in the WGEW.

and porosity, two of the more influential soil parameters. These supplemental maps have also been employed as input to the Noah LSM in this work.

[14] In addition to these "standard" soils data sets, which are based on large groupings of soil pedon data collected at many locations not necessarily representative of the WGEW soils, the WGEW has also been the subject of several field campaigns in which in situ soil texture and hydraulic property data were collected. During the M90 experiment, soil texture estimates at each Metflux site are as given by *Schmugge et al.* [1994]. Table 2 of *Santanello et al.* [2007] cites estimates from a neural network-based PTF (ROSETTA) [*Schaap et al.*, 1998], measurements made during 2002 (M. G. Schaap and P. J. Shouse, personal communication, 2004, as cited by *Santanello et al.* [2007]) (hereinafter Schapp and Shouse, personal communication, 2004) and the 2004 North American Monsoon Experiment (NAME) [*Higgins et al.*, 2006]. In this work, we employ comparisons with the 2002 measurements of Schaap and Shouse (personal communication, 2004) because all of the soil hydraulic properties required for the Noah LSM were provided at sites 1 (Lucky Hills) and 5 (Kendall).

2.4. Meteorological Data

[15] For the simulations in this study, the input forcing from solar and long-wave radiation, temperature, humidity, wind speed, and surface atmospheric pressure were obtained by a merger of data sets from the available sites in the WGEW, due to the noncentered locations of the Metflux sites as well as several sites having discontinuous observations, and are applied as spatially constant values throughout the watershed. The precipitation data set collected at 84 precipitation gauges throughout the watershed (as shown in Figure 2) is aggregated from breakpoint data to hourly intervals and then interpolated spatially over the watershed following the multiquadric-biharmonic method described by *Garcia et al.* [2008]. As shown in Figure 2, the eight M90 Metflux sites are either collocated with (sites 1, 3, and 5–8), or situated very near (sites 2, 4, and 8), a precipitation gauge. For those sites without a collocated precipitation gauge (gauges 2, 4, and 8), the interpolated field is employed in order to determine the precipitation intensity at those locations.

[16] Several methods for degradation of the forcing precipitation were employed to produce alternative data sets for input to the LSM, in order to examine the sensitivity of the parameter estimation process (described below) and the resulting soil moisture values to the quality of the input precipitation data set. One method employed here was application of the watershed mean-areal precipitation (MAP) based on the interpolated field over the entire WGEW at each hour. This method is thought to preserve some information from the actual spatial distribution of the precipitation in the watershed during the study period, whereas a simple average of all gauges in the watershed removes all such information from the resulting MAP value. For example, during the study period examined here, the MAP value found by simple mathematical averaging of the WGEW gauges gives a total-period value of 31.2 mm, whereas spatial averaging of the interpolated field produces a total-period MAP value of 40.6 mm (see Figure 3). This difference can be attributed to the limited spatial extent of the convective precipitation observed during the M90 period, as discussed by *Garcia et al.* [2008].

[17] Another method for degradation of the input precipitation data set simply took the precipitation measured at a single gauge near the center of the watershed (gauge 33, indicated in Figures 2 and 3) for application over the entire WGEW, as studies suggest that a single gauge is likely the only instrumentation available in a typical area similar to the size of the WGEW ($\sim$150 km^2) throughout much of the United States [see *Garcia et al.*, 2008]. This particular gauge was selected for its central location within the WGEW as well

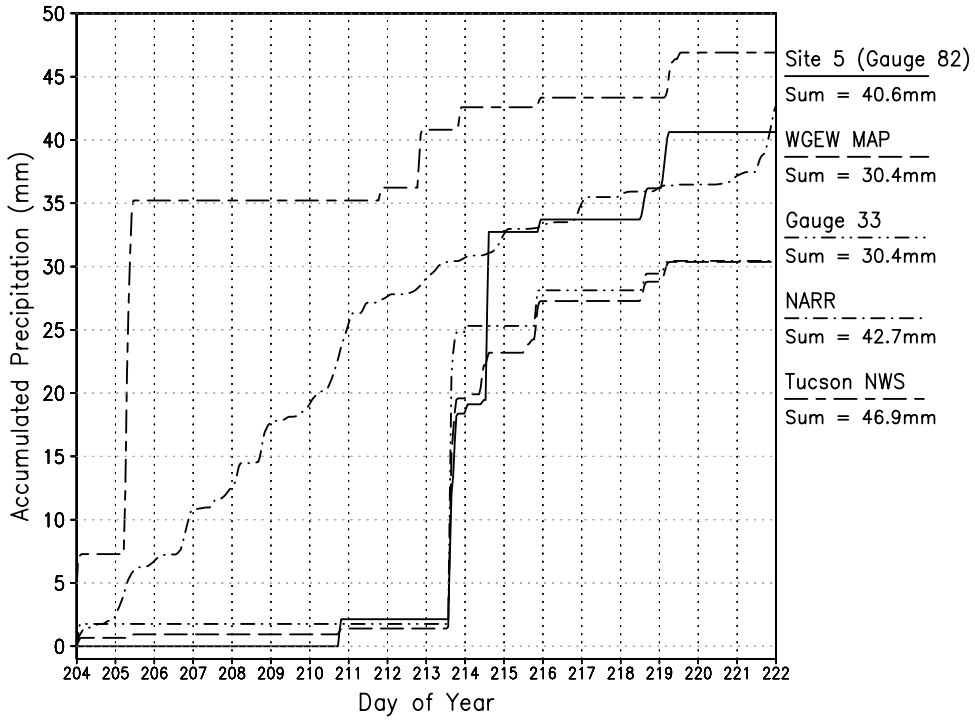

Figure 3. Accumulated precipitation from the various forcing data sets used in this work.

as coverage of its location in the PBMR observations during the M90 experiment.

[18] One additional choice for a single-gauge source of precipitation data for the period of interest was selected: the nearest first-order NWS location is located approximately 100 km distant from the WGEW in Tucson, Arizona. For a study location similar to the WGEW but without resources provided by the SWRC, and especially during the M90 experiment, it is more likely that information on meteorological conditions will come from outside of the study region entirely. The selection of the Tucson precipitation gauge as a proxy source of information is intended to represent that likelihood.

[19] One final method employed precipitation values in the region of the WGEW as provided in the one-third-degree North American Regional Reanalysis (NARR) [*Mesinger et al.*, 2006]. The NARR data set shows consistently light and moderate, but not intense, precipitation during the M90 experiment over the WGEW area. However, such small precipitation rates and totals were not observed in the WGEW, and the results provided by the NARR may be attributed to the large region of focus in that work. However, we considered that, in the absence of even first-order NWS stations, data sets like the NARR may provide the best information that can be obtained for many regions about the world, and are similar in format and detail to output from a numerical forecast model.

[20] The cumulative time series of precipitation from these sources, compared with that observed at the site 5 (precipitation gauge 82) Metflux location, are shown in Figure 3. The precipitation estimates based on gauges within the WGEW show little precipitation until late on 1 August 1990 (DOY 213), when a very intense event occurred. The precipitation intensity during this event varied between the data sets, however. The NARR data set significantly underestimated the event intensity and the Tucson gauge did not capture this event at all, while the center-gauge records show slightly more intense precipitation during this event. Following the analysis provided by *Garcia et al.* [2008], this event was likely convective in nature and was focused on a portion of the WGEW that included the center gauge, providing the higher total precipitation there while much of the remainder of the watershed was less affected by the storm, producing a slightly lower MAP estimate for the event.

[21] As a positive result of these input selections, the MAP estimates seem to capture most of the small events that occurred during the study period, such as those on 3 August (DOY 215) and 6 August 1990 (DOY 218). Overall, the NARR input data show more frequent, low-intensity precipitation events throughout the study period, especially prior to 1 August 1990 (DOY 213) while the WGEW was predominantly dry. The Tucson gauge recorded an intense event on 24 July 1990 (DOY 205) that is not found in the WGEW observations, and then only small events through the remainder of the study period. A complete lack of precipitation signal at the Tucson gauge on 1 August 1990 (DOY 213) reinforces the conclusion that the precipitation event on that day remained localized over and near the WGEW.

[22] All of the gauge-based estimates in the WGEW demonstrate a dry period between 25 July (DOY 206) and 29 July 1990 (DOY 210). The Tucson gauge shows the highest total amount of precipitation over the study period, and the NARR total is the second highest over the period but with a distinctly different profile from that observed at gauge locations. The WGEW MAP and center-gauge estimates demonstrate the least total rainfall over the study

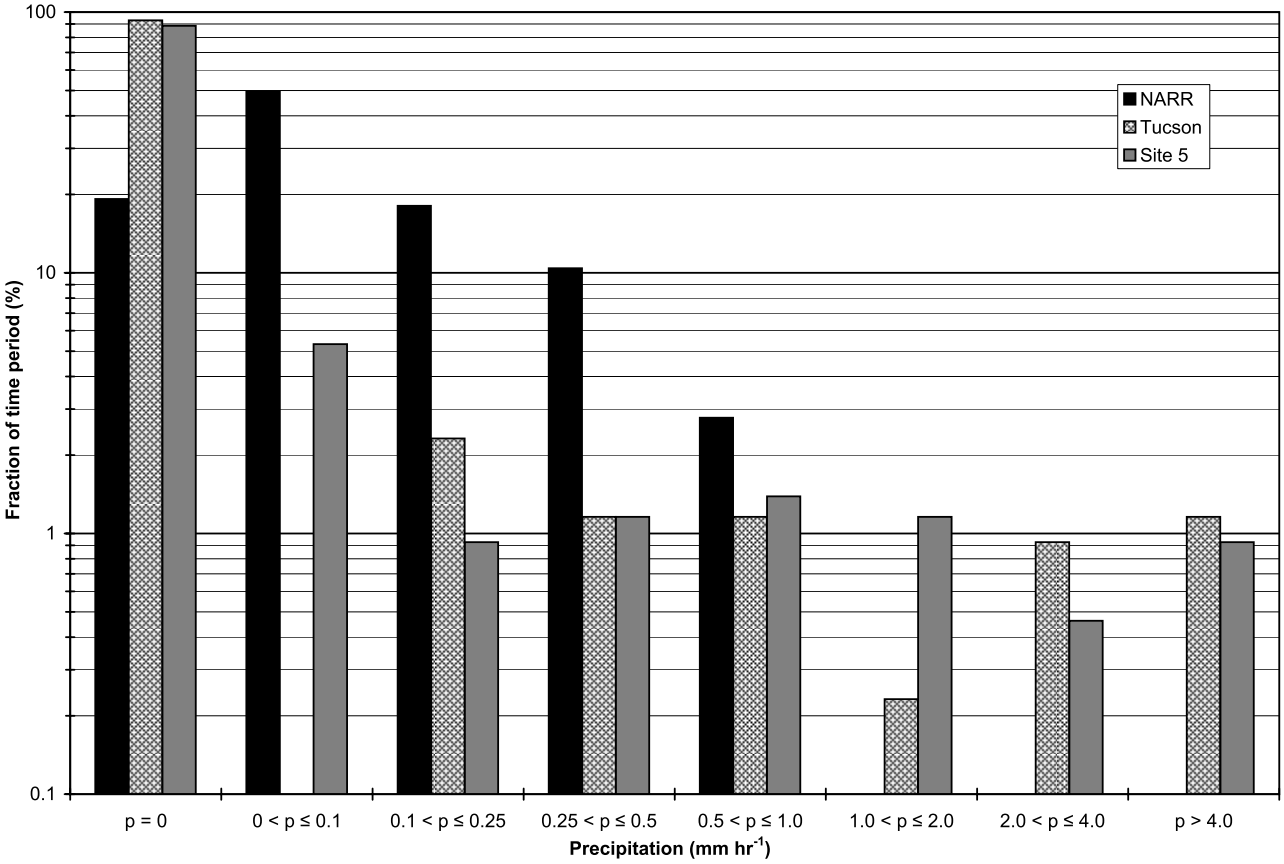

Figure 4. Probability density functions of hourly precipitation rate (p) from the NARR reanalysis, the Tucson NWS gauge, and the WGEW precipitation gauge (gauge 82) at site 5.

period of those input data sets considered here, and remain close to each other in both magnitude and profile. The total precipitation measured by the gauge at site 5 is nearly 10 mm greater than the MAP or center-gauge based estimates. It should be noted that additional storm event information is captured at this site on 29 July (DOY 210), 2 August (DOY 214), and 6–7 August 1990 (DOY 218–219).

[23] Another representation of the differences between the selected precipitation data sets may be shown by probability density function (PDF) of hourly precipitation rates within selected ranges, as shown in Figure 4. This analysis shows that, for a significant portion of the study period, no precipitation was recorded by surface gauges in or near the WGEW. However, the NARR analysis suggests that nonzero precipitation occurred over nearly 80% of the study period, though significant portions of the NARR precipitation occurred with intensity at or below the measurement accuracy of the precipitation gauge stations (0.25 mm). We attribute this result to the relatively coarse (one-third degree) horizontal spatial resolution of meteorological variables generated by the NARR model. The NARR also demonstrates a greater frequency of precipitation rates below 1 mm hr^{-1} than did the precipitation gauges or their derivative measures, and did not contain any occurrences above 1 mm hr^{-1} in intensity. The PDF analysis suggests that the observations obtained at the Tucson and site 5 gauges were similar in their patterns of intensity, though the Tucson gauge recorded greater frequencies of both heavy rainfall and dry periods than the site 5 gauge (gauge 82).

3. Background and Approach

[24] As mentioned above, this work builds upon and extends the work of *Santanello et al.* [2007], which includes more extensive discussions of the model soil physics, parameter estimation, and the methodology specific to soil hydrologic parameter and texture estimation. Below, we provide a brief summary of this background material in order to support our experimental approach in this work.

3.1. Soil Moisture Physics in Land Surface Models (LSMs)

[25] The influence of near-surface soil moisture on the partitioning of surface turbulent fluxes of moisture and latent and sensible heat to the atmosphere, using both offline LSMs and fully coupled land–atmosphere models, has been documented in numerous studies [e.g., *Cuenca et al.*, 1996; *Santanello and Carlson*, 2001; *Ek and Holtslag*, 2004]. In order to simulate properly the evolution of moisture distribution in the soil column, a set of soil hydraulic parameters is combined with characteristic curves that relate soil moisture with both matric potential and hydraulic conductivity. The expressions derived by *Brooks and Corey* [1964] and *Campbell* [1974] have been commonly used in coupled meteorological models, along with parameter lookup tables based on the results of soil studies by *Clapp*

and Hornberger [1978], *Rawls et al.* [1982], *Cosby et al.* [1984], and numerous others. A full survey of these functions has been provided by *Braun and Schadler* [2005].

[26] High-resolution soil texture maps such as the SSURGO data set remain difficult to obtain, especially on regional and global scales. Often, there is little or no variability indicated for a singular or mixed soil type due to a dearth of data, despite observations of greater variation in soil properties within certain soil types than between types [*Feddes et al.*, 2003; *Soet and Stricker*, 2003; *Gutmann and Small*, 2005]. To bridge the conceptual gap between commonly used soil texture classes and the heterogeneous nature of individual soil types, numerous pedotransfer functions (PTFs) have been developed [*Cornelis et al.*, 2001; *Sobieraj et al.*, 2001]. Though the advantages of continuous PTFs over class-oriented systems have been demonstrated for hydrologic models [*Soet and Stricker*, 2003], continuous PTFs are not routinely employed in LSMs, and the broad definitions of soil types as classes still dominate the simulation of soil moisture dynamics in application.

3.2. Parameter Estimation Methodology

[27] An alternative to the uncertain specification of soil hydraulic parameters by class-oriented methods in LSMs is the use of parameter estimation and model calibration methods. One relatively simple, model-independent and well-established framework, the Parameter Estimation Tool (PEST) [*Doherty*, 2004], has been used in a number of scientific disciplines for parameter optimization given limited observations of the fundamental output variables. For example, in application to this work, one can adjust the soil porosity defined for the LSM until the differences over time between simulated and observed soil moisture values are minimized. By the specification of convergence limits and an objective evaluation function, for single or numerous variables and parameters of interest, PEST is able to perform such adjustments until an optimum solution for the desired parameter set is found. For the experiments described below, an objective function based on the RMSE of the simulated soil moisture (in comparison with the PBMR observations) is specified.

[28] More sophisticated estimation methods have recently been developed to estimate large and diverse sets of parameters. *Liu et al.* [2003] used a multiobjective technique for offline LSMs and partially coupled land-atmosphere models to examine the ways by which deficiencies in the model physics can impact coupled and decoupled simulations. Following this work, *Liu et al.* [2005] performed controlled parameter estimation studies of offline and partially coupled models and examined the impact of including atmospheric parameters, in addition to the usual soil and vegetation parameters, in the optimization. *Hogue et al.* [2005] investigated the transferability of optimized parameter sets from an offline LSM to alternative surface conditions and time periods, and concluded that parameter optimization needs to be site-specific for best results and that recalibration for changes in seasons or over long simulation periods may be required.

[29] *Scott et al.* [2000] estimated soil hydraulic parameters using the Hydrus soil moisture model at two sites in the WGEW. While their focus remained on the vertical distribution of soil moisture and recharge at individual points, their results demonstrated that the model employed was less sensitive to the value of saturated hydraulic conductivity than to the values of porosity and pore size distribution index, which are consistent with other studies. Scott et al. also emphasized that the derived values are "effective" and compensate for errors in the model's representation of the real soil physics, and that further research is needed to assess the limitations of parameter estimation across spatially distributed, heterogeneous watersheds.

[30] In this work, we explore two approaches to the estimation of soil hydraulic parameters. In one approach, the hydraulic parameters are estimated directly in a manner similar to the studies described above; this approach is denoted below as "PEST-Direct." In the second approach, the *Cosby et al.* [1984] PTF (described below) is employed as an additional constraint on the parameter estimation process. This yields an estimate not only of the soil hydraulic properties but also of the soil texture, which is useful for other applications that depend on the texture information. This method, denoted below as "PEST-PTF," is described in more detail in the following section.

3.3. Estimation of Soil Hydraulic Parameters and Texture

[31] *Santanello et al.* [2007] demonstrated that aircraft-based radiometric observations of near-surface soil moisture could be combined with the Noah LSM using PEST, within the LIS simulation framework, to estimate soil hydraulic parameters that compared reasonably well to the various in situ estimates for the WGEW, as referenced above. Because that study employed the PTF established by *Cosby et al.* [1984], which is consistent with the assignment of hydraulic parameters according to the soil classes currently employed in the Noah LSM, useful byproducts of the soil hydraulic property estimation are simultaneous estimates of sand, silt and clay content which, when combined, provide an overall estimate of soil texture. The Cosby et al. PTF models the hydraulic parameters as follows:

$$\theta_s = 0.489 - 0.00126*\mathrm{SAND}, \tag{1}$$

$$\psi_s = \frac{10.0 \exp[1.88 - 0.0131*\mathrm{SAND}]}{100.0}, \tag{2}$$

$$K_s = \frac{0.0070556*10.0 \exp[-0.884 + 0.0153*\mathrm{SAND}]}{1000.0}, \tag{3}$$

$$b = 2.91 + 0.159*\mathrm{CLAY}, \tag{4}$$

where θ_s is the porosity ($m^3\ m^{-3}$), ψ_s is the saturated or air-entry matric potential (m), K_s is the saturated hydraulic conductivity ($m\ s^{-1}$), b is the inverse of the pore size distribution index, and SAND and CLAY are specified as percentages of the soil sample. This PTF yields soil hydraulic properties as continuous functions, in contrast to the typical approach of LSMs in which lookup tables contain average values for discrete soil texture classes. Given that the functional form of the PTF is appropriate for a particular location, the use of a PTF provides an additional constraint on the soil hydraulic parameter estimation that forces the estimated hydraulic properties to converge in a more physically consistent manner.

Table 1. Mean Bias of the Top 5-cm Volumetric Soil Moisture Between Noah and the PBMR Observations, Averaged Over the Six PBMR Times at All Eight Metflux Sites, for the Simulations With Varied Soil Texture Data Sets and PEST[a]

Soils	Site 1	Site 2	Site 3	Site 4	Site 5	Site 6	Site 7	Site 8
FAO	3.054	1.372	2.172	1.276	2.254	1.749	3.838	4.087
STATSGO	2.524	0.891	1.666	0.851	1.699	1.331	3.345	3.578
SSURGO -N/C	3.384	4.272	4.896	1.276	5.759	1.854	6.679	4.501
SSURGO -K/P	−1.029	4.671	3.608	−1.806	4.434	−2.088	7.082	−3.319
PEST-Direct	−0.141	−0.371	0.091	−0.036	−0.072	−0.140	0.371	0.082
PEST-PTF	0.105	−0.389	0.338	0.057	0.189	0.192	1.126	0.432

[a]Volumetric soil moisture is given as percent.

[32] As in work by *Santanello et al.* [2007], the PEST objective function employed in this study is the root-mean-square error (RMSE) of the simulated volumetric soil moisture, compared against the PBMR observed soil moisture, both of which represent a 5-cm layer average. The calibration was performed independently on a point-by-point basis at each of the eight Metflux sites shown in Figure 1.

3.4. Experimental Design

[33] An alternative to the PEST-PTF approach described above, and that most commonly employed in previous studies, is the direct estimation of hydraulic parameters using PEST. On the basis of the discussion above, one might expect that this ''PEST-Direct'' approach would result in smaller RMSE than the PEST-PTF approach, but because the PTF constraint is not employed, the PEST-Direct approach could estimate hydraulic properties that are physically inconsistent with a single soil texture. Accordingly, one of the first objectives of this study is to compare the performance of the PEST-Direct and PEST-PTF approaches to the estimation of soil hydraulic parameters by comparing these simulation results with in situ hydraulic property estimates.

[34] In addition to the comparison of PEST methods, the second major objective of this study is to examine the role of precipitation uncertainty in the soil parameter estimation process. In order to do this, as described above, we incorporate various precipitation estimates of differing accuracy for the WGEW during the M90 experiment.

[35] In order to conform to the spatial resolution of PBMR soil moisture products obtained during the M90 experiment, as described above, the simulation system was configured with 40-m horizontal grid spacing over the WGEW. Simulations were begun at 00 LST on 23 July 1990 (DOY 204) and continued to 00 LST on 10 August 1990 (DOY 222). At the start of each model simulation, the Noah LSM was configured to calculate the maximum allowable time step for numerical stability in the soil moisture dynamics, based on the soil parameters to be used. The typical time step was calculated as 5–6 minutes, depending on the soil type estimates a priori at the simulated point. Hourly meteorological and precipitation forcing values were linearly interpolated to the necessary time step in the course of the simulation.

[36] The Noah LSM was configured with four soil layers of 5-, 35-, 60-, and 100-cm thicknesses for a total soil column depth of 2 m. The initial soil moisture at all levels in the profile was set to that obtained from the PBMR observations for the surface layer, and the initial soil temperature at all levels in the profile was set to 293 K, which was near the observed air temperature at the initial time. The temperature at the bottom of the soil column in the Noah LSM was set to 286.5 K and remained constant over the course of the simulation, and no water was present on the vegetation at the initial time. The topsoil layer thickness of 5 cm was chosen in order to replicate the penetration depth of the PBMR observations and the in situ gravimetric measurements. In addition to the soils and precipitation data sets described above, the land cover and vegetation parameters for the Noah LSM in the simulation system were derived from the 1992 North American Landscape Characterization (NALC) [*Lunetta and Sturdevant*, 1993] data set, along with climatological values for surface albedo (derived on a quarterly basis) and vegetation greenness fraction (derived on a monthly basis) from those employed in operational use of the Noah LSM at the NOAA-NWS National Centers for Environmental Prediction [*Ek et al.*, 2003].

[37] In order to duplicate the results presented by *Santanello et al.* [2007], we first executed the simulation system at each of the eight Metflux sites shown in Figure 1 using the four different soils data sets described above, without soil texture calibration. We then executed these simulations using the PEST-based soil texture optimization by the two methods described above. Following these experiments, the precipitation at each site was systematically varied using the different estimates described above. The collection of these experiments is intended to demonstrate the impact of precipitation uncertainty on estimates of soil texture by way of the simulated surface soil moisture results. Finally, we demonstrate the impact of precipitation uncertainty on simulated surface soil moisture results while calibrating both soil texture and a particular parameter of the Noah LSM formulation for evaporation from bare soil.

4. Results

[38] The experiments conducted for this work focus first on the PEST-Direct and PEST-PTF approaches to soil hydraulic parameter estimation, using all the available precipitation data for the WGEW. Following these experiments, we examine the role of precipitation uncertainty in soil parameter estimation, including the tradeoffs between infiltration- and evaporation-related soil parameters.

Table 2. Mean RMSE of the Top 5-cm Volumetric Soil Moisture Between Noah and the PBMR Observations, Averaged Over the Six PBMR Times at All Eight Metflux Sites, for the Simulations With Varied Soil Texture Data Sets and PEST[a]

Soils	Site 1	Site 2	Site 3	Site 4	Site 5	Site 6	Site 7	Site 8
FAO	3.858	2.341	3.029	1.628	2.517	2.371	4.298	4.688
STATSGO	3.331	1.906	2.609	1.214	1.959	1.997	3.822	4.151
SSURGO-N/C	4.286	5.529	5.741	1.628	6.280	2.455	7.275	5.206
SSURGO-K/P	1.865	5.996	4.432	2.247	4.867	2.519	7.726	4.258
PEST-Direct	1.057	1.126	1.756	0.631	0.372	1.041	1.655	1.293
PEST-PTF	1.660	1.174	1.985	0.710	0.978	1.385	2.527	1.518

[a]Volumetric soil moisture is given as percent.

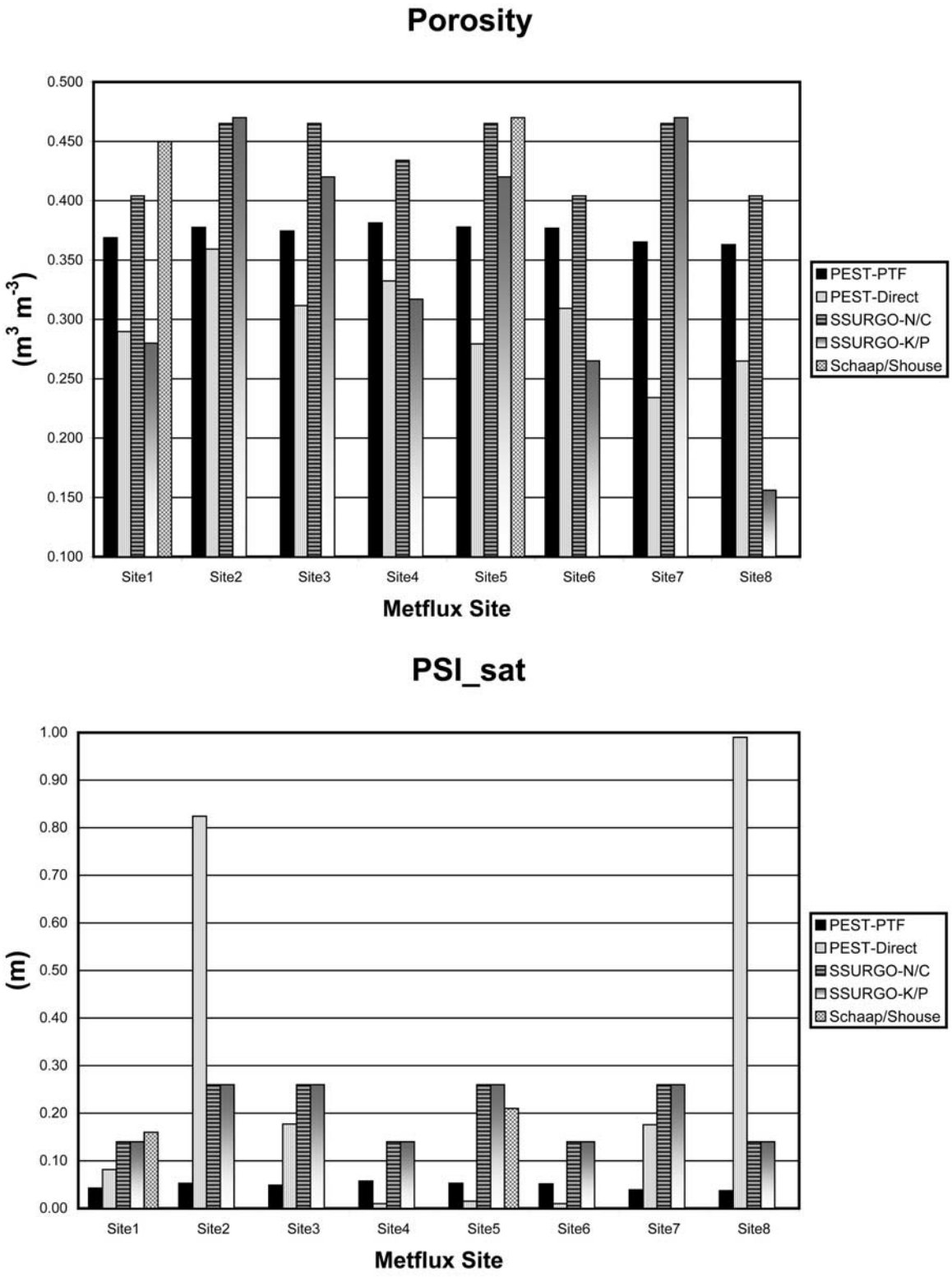

Figure 5. Values of soil hydrologic parameters estimated from the PEST-PTF and PEST-Direct simulations at all eight Metflux sites in the WGEW, compared with values from the SSURGO soil survey and in situ measurements by Schaap and Shouse (personal communication, 2004). Details on the SSURGO data set can be found in the text. The Schaap and Shouse measurements were taken only at Sites 1 and 5.

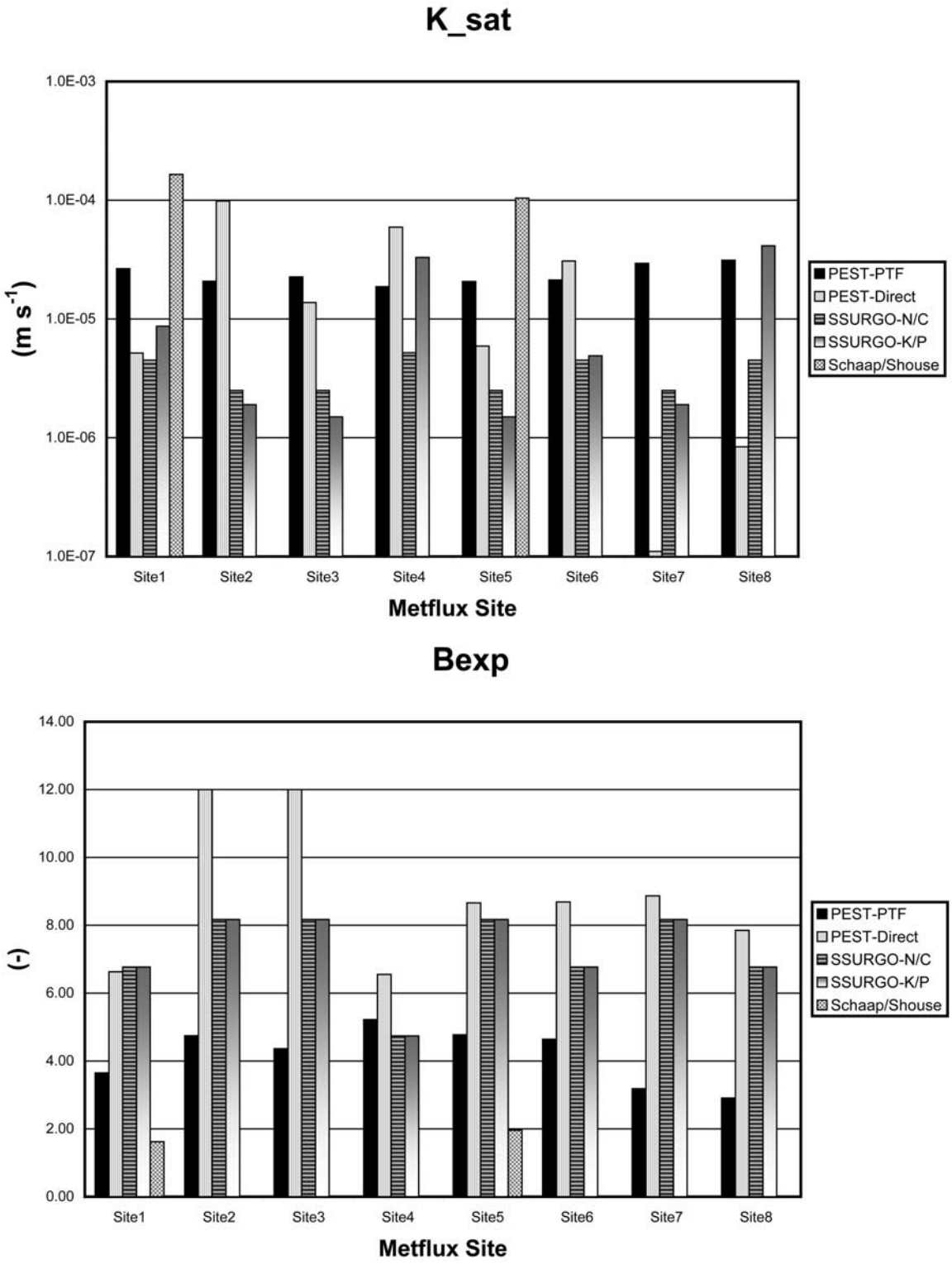

Figure 5. (continued)

4.1. PTF-Constrained Versus Direct Soil Property Estimation

[39] The bias and RMSE for the simulated volumetric soil moisture at all eight Metflux sites in the WGEW, relative to the six PBMR measurements obtained during the M90 experiment, are shown in Tables 1 and 2, respectively. For the FAO, STATSGO, and SSURGO-N/C cases (where N = Noah and C = Cosby) listed there, the soil texture class for each site is taken directly from the indicated source map. The standard Noah LSM soil parameter lookup table, based on the average values from *Cosby et al.* [1984], is then used to specify soil hydraulic and thermal parameters for a given texture class.

Table 3. Mean Bias of the Top 5-cm Volumetric Soil Moisture Between the PEST-PTF Method and the PBMR Observations, Averaged Over the Six PBMR Times at All Eight Metflux Sites, for the Simulations With Varied Precipitation Forcing[a]

Precipitation	Site 1	Site 2	Site 3	Site 4	Site 5	Site 6	Site 7	Site 8
Interpolated	0.105	−0.389	0.338	0.057	0.189	0.192	1.126	0.432
WGEW MAP	0.826	−0.236	0.133	−0.148	−0.379	−0.141	1.663	0.614
Gauge 33	0.005	−0.361	0.090	−0.089	−0.330	−0.141	0.809	0.396

[a]Volumetric soil moisture is given as percent.

[40] For the SSURGO-K/P case (where K = K_s and P = θ_s = porosity), the SSURGO soil texture map is used with the Noah LSM lookup table for all soil parameters except the saturated hydraulic conductivity (K_s) and the porosity (θ_s), which are given in the SSURGO data set. It is recognized that these cases employ sets of soil hydraulic parameters that may not be physically consistent, as the SSURGO values for these parameters for a given soil may not be near those given in the Noah LSM lookup table for soils in the same texture class. Resulting differences in the optimized soil texture are meant to demonstrate the inconsistency in such a combination of data from disparate sources. While a PTF approach is intended to produce parameter values for a given soil texture that are physically consistent within the set, simple substitution of lookup table value with those given in the SSURGO data set is not necessarily a proper approach unless all of the necessary parameter values are provided, ensuring that same physical consistency.

[41] The final cases listed in Tables 1 and 2 indicate the parameter estimation methodologies described above: PEST-Direct and PEST-PTF. It is consistent with the results of *Santanello et al.* [2007] that, by using all six PBMR observations during the M90 experiment for calibration of the soil hydraulic parameters, the PEST-Direct and PEST-PTF cases demonstrate the smallest bias and lowest RMSE among the various cases at all eight Metflux sites in the WGEW. As shown in Table 2, the use of PEST by either method in order to calibrate the soil texture at each site results in an RMSE of 1.5% or less, compared to approximately 4% using standard soil classes from the FAO, STATSGO, or SSURGO maps and the default values provided in the Noah LSM. Tables 1 and 2 confirm the expected result that the PEST-Direct approach yields slightly lower bias and RMSE values than the PEST-PTF approach. The average difference in soil moisture RMSE is 0.4% volumetric, which is well within the uncertainty of the observations. This result suggests that the two approaches are essentially equivalent with respect to soil moisture prediction error.

[42] Figure 5 shows a comparison of the soil hydraulic properties estimated via the PEST-PTF and PEST-Direct approaches at the eight WGEW Metflux sites, the "standard" SSURGO-based estimates, and the in situ estimates of Schaap and Shouse (personal communication, 2004). As described above, the SSURGO-N/C values are derived from the SSURGO soil texture maps for WGEW referenced to the Noah LSM lookup tables. The SSURGO-K/P values are the same as SSURGO-N/C for the air-entry pressure (PSI_sat) and the pore size distribution index (Bexp) while the porosity and saturated hydraulic conductivity (K_sat) are derived from the SSURGO mapping unit data based on pedological analysis.

[43] As shown in Figures 5a and 5b, the in situ estimates of porosity and K_sat at sites 1 and 5 suggest that the PEST-PTF provides superior estimates of these properties when compared with the results of the PEST-Direct approach. In addition, it is interesting to note that the SSURGO-N/C estimates are the closest to the in situ estimates for porosity and K_sat despite the results shown in Tables 1 and 2, in which the SSURGO-N/C results produce the highest soil moisture prediction bias and RMSE for all sites. This appears to be related to differences in the other two hydraulic parameters, shown in Figures 5c and 5d. Figures 5a and 5b also show that the PEST-PTF method yields porosity and K_sat estimates that are consistently closer to the SSURGO-N/C estimates than those estimated by the PEST-Direct approach.

[44] Estimates of the other two hydraulic parameters are shown in Figures 5c and 5d. The PEST-PTF and PEST-Direct estimates for the air-entry matric potential PSI_sat at sites 1 and 5 produce mixed results. The PEST-Direct results at site 1 are closer to the in situ observations, while the PEST-PTF results are closer at site 5. The behavior of PEST-Direct at sites 2 and 8 is particularly suspect, and underscores the issue discussed previously that the direct approach may yield parameter combinations that are inconsistent with a single soil texture. The PSI_sat estimates at other sites also produce mixed results with respect to the SSURGO values. The Bexp results at sites 1 and 5 are consistent with those for porosity and K_sat, in which the PEST-PTF approach appears to provide estimates closer to the in situ observations. In addition, the PEST-PTF results are consistently lower than the SSURGO results for Bexp.

[45] The Bexp and PSI_sat results may explain the somewhat counterintuitive result that the PEST-PTF approach yields significantly lower soil moisture prediction errors than the use of SSURGO parameters, despite the similarities in their estimated porosity and saturated hydraulic conductivity values. This suggests the critical role that the other hydraulic properties can play in soil moisture prediction. Overall, these results highlight the importance of the PTF constraint on estimation of hydraulic parameters as a physically consistent set, rather than individually. While the PEST-Direct approach can be more accurate for a few individual sites and parameters, the hydraulic parameters at each site can be inconsistent with one another and, as a set, would correspond to a soil texture that is physically unrealistic.

4.2. Precipitation Uncertainty

[46] Considering the results presented in the previous section, further simulations oriented on exploration of the role of precipitation uncertainty in the parameter estimation

Table 4. Mean RMSE of the Top 5-cm Volumetric Soil Moisture Between the PEST-PTF Method and the PBMR Observations, Averaged Over the Six PBMR Times at All Eight Metflux Sites, for the Simulations With Varied Precipitation Forcing[a]

Precipitation	Site 1	Site 2	Site 3	Site 4	Site 5	Site 6	Site 7	Site 8
Interpolated	1.660	1.174	1.985	0.710	0.978	1.385	2.527	1.518
WGEW MAP	2.570	1.155	1.453	0.915	1.411	1.127	2.307	1.733
Gauge 33	1.953	1.142	1.447	1.168	1.616	1.486	2.154	1.354

[a]Volumetric soil moisture is given as percent.

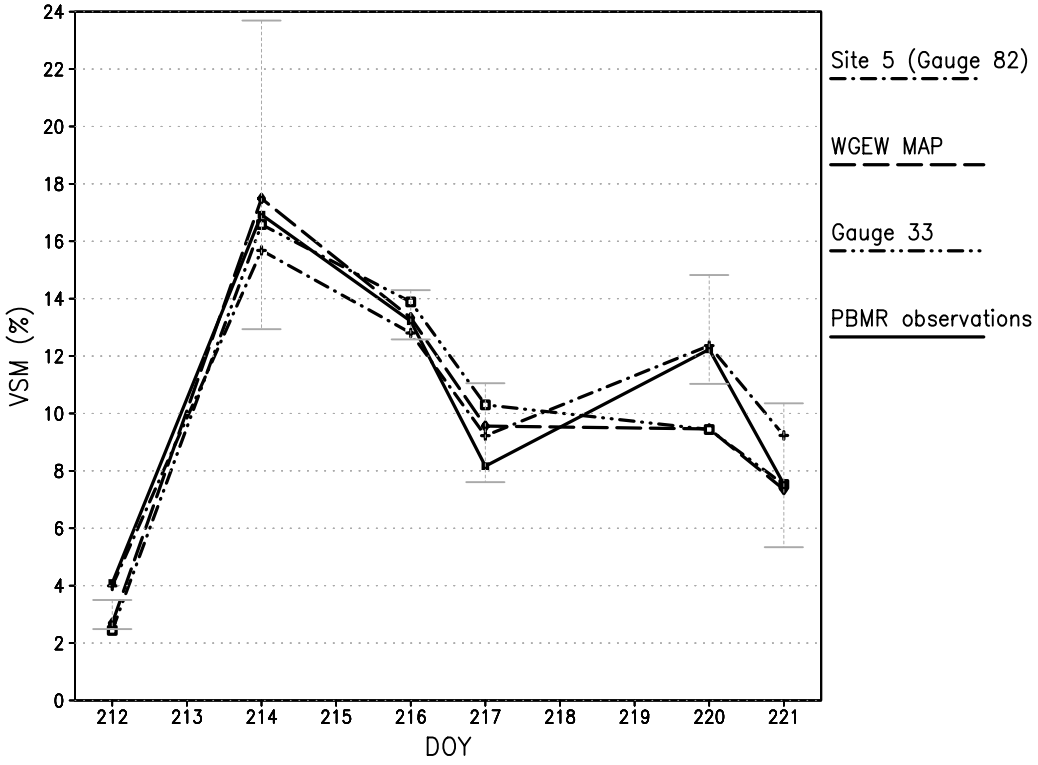

Figure 6. Simulated and observed near-surface soil moisture at WGEW site 5 for the precipitation sensitivity experiments.

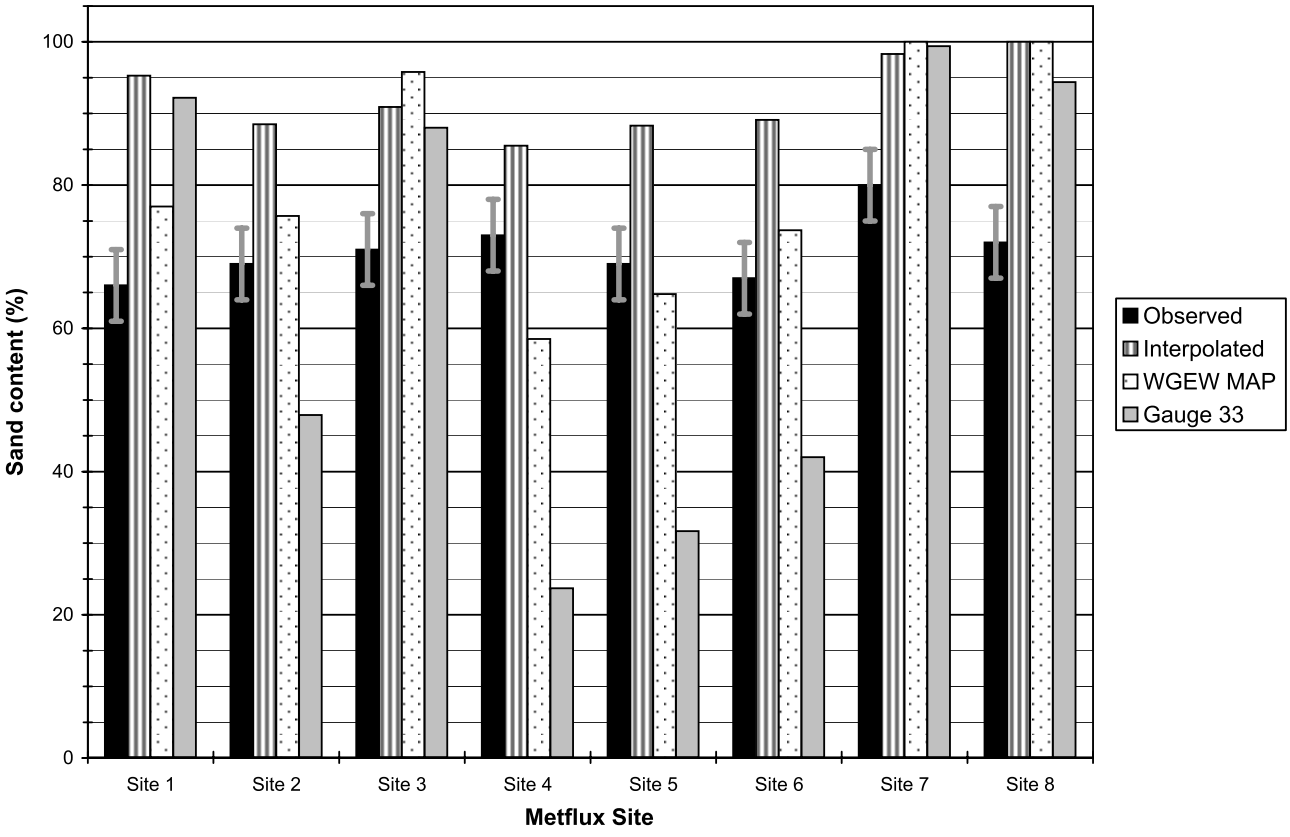

Figure 7. Observed and estimated soil sand content at the eight WGEW Metflux sites during the M90 experiment.

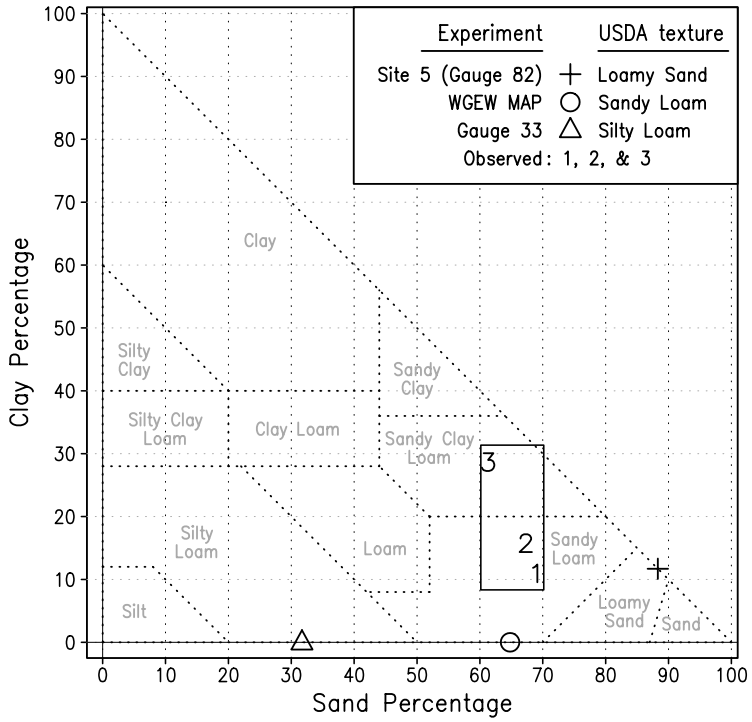

Figure 8. Final PEST-estimated sand-clay-silt content for the precipitation uncertainty simulations at site 5, depicted on the USDA soil texture triangle.

process have employed the PEST-PTF approach to estimate soil textures and associated hydraulic properties. Similar to Tables 1 and 2 above, simulated surface soil moisture bias and RMSE values at the eight Metflux sites in the WGEW under the described variety of precipitation forcing are listed in Tables 3 and 4, respectively. Generally, the biases are smaller and the RMSE values are lower than in Tables 1 and 2, indicating that the PEST-PTF approach to estimation of the soil textures and hydraulic parameters is more important to accurate simulation of the surface soil moisture than the use of the best possible precipitation forcing, provided that the forcing is based on information from observations (gauge values, not modeling or reanalysis results) at a nearby location (within the WGEW in this case, not from a distance of nearly 100 km). In short, the best results are produced in simulations that employ forcing data based on local observations, an intuitive and physically consistent result.

[47] It is for this reason that we note another important result: simulations that employed precipitation forcing from the Tucson and NARR sources were unable to converge upon an optimized solution for soil hydrologic properties using either the PEST-Direct or PEST-PTF approaches. This result underscores the necessity of having at least one precipitation gauge in the immediate area of interest in order to produce a viable estimate of soil texture parameters and reasonable soil moisture results. Even with six PBMR-derived soil moisture images available for comparison and calibration over the simulation period, the precipitation intensity and temporal patterns in the records from those two sources were highly inconsistent with the observed precipitation at the WGEW sites. This inconsistency was so great that the proper simulation of the observed soil moisture in the WGEW, within the limits of our specified soil moisture RMSE objective function, was impossible, regardless of the extent to which PEST was allowed to adjust the soil textures and hydraulic parameters employed in the Noah LSM.

[48] As shown in Figure 3, the NARR and Tucson precipitation totals are approximately 43% and 56% greater, respectively, than those over the watershed for the period, and their temporal profiles are also significantly different from those records observed in the WGEW itself. In addition, Figure 4 shows that the precipitation rate PDFs from both sources are quite different from those observed in the WGEW. A large event in Tucson in the early dry period that was not also observed in the WGEW, and the tendency for the NARR data set to produce consistent low-intensity rainfall with few heavy events, contribute to the inability of PEST to produce a solution using these inputs. Because the M90 period was one of highly convective and therefore localized precipitation, it would be expected that precipitation events and regimes with a higher spatial or temporal correlation would be more likely to produce viable soil hydrologic parameter estimates using synoptic or mesoscale analyses and networks. The results suggest that it is also important to capture the correct range of precipitation intensity in order to evaluate the ability of the LSM to correctly simulate soil drying after each event, as controlled by both hydraulic and hydrologic properties. Other quality-based characteristics of the precipitation record that may be required for successful optimization results are discussed below.

[49] Figure 6 shows the simulated and observed volumetric soil moisture (VSM, often expressed in $m^3\ m^{-3}$ or percent) at the six PBMR observation times, as well as the time series of simulation bias, at site 5. The error bars on the plot indicate the standard deviation of observed in situ

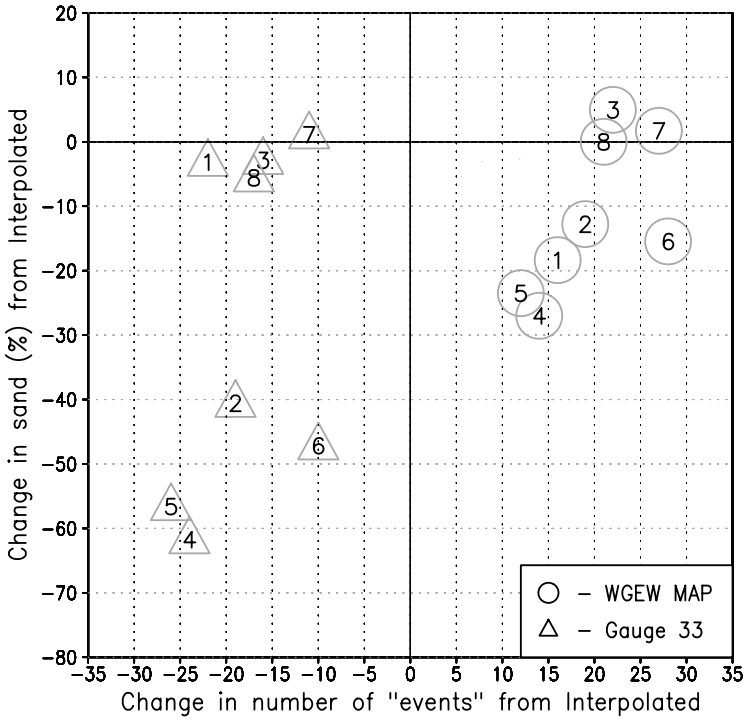

Figure 9. Scatterplot of the change in the number of precipitation "events" (defined here as the number of hours in the time series with measurable precipitation) versus the change in the PEST-estimated sand content.

(gravimetric) values at the same times, although it should be noted that the gravimetric averages upon which these error bars are centered are close, but not exactly equal, to the PBMR values at each observation time. This figure highlights the changing sensitivity of both simulated and observed soil moisture values to precipitation inputs over time: the results remain quite similar during the initial dry period and following the large event on 2 August 1990 (DOY 214), but then diverge during the dry period after 6 August (DOY 218). This indicates that events measured at other precipitation gauges in the network, but not at site 5, may contribute to large errors in some of the simulation results that occur outside the range of observed soil moisture on 8 August (DOY 220). Despite the accuracy of the input precipitation forcing, the simulated soil moisture remains too high through the end of the simulation. This result may be due in part to errors in the specification of evaporation parameters for bare soils, as discussed below.

[50] It is clear from Tables 3 and 4 that the optimization procedure using PEST for determination of soil textures produces results superior to the use of the default Noah LSM lookup tables based on coarse specification of soil texture classes, no matter which watershed-based rainfall estimate is used. However, we also wish to determine whether these results are physically realistic, and whether that realism decreases with the accuracy of the precipitation input. Figure 7 demonstrates the impact of selected precipitation records on the estimated sand content of the soil column, as derived using the PEST-PTF approach. The complete sand-silt-clay observations collected during the M90 experiment [*Schmugge et al.*, 1994] are listed in Appendix A.

[51] As shown in Figure 7 and Table A1, the tendency of this approach is to estimate values of sand content that are too high, and also to estimate little or no silt content in the soil column. This apparent lack of silt content is a direct consequence of the *Cosby et al.* [1984] PTF in equations (1)–(4), which depend on only the sand and clay content of the soil column. Therefore, we must conclude that any sensitivity to silt is indirect in this work, and the opportunity exists for extension of this work with other PTFs that may take into account the full heterogeneity of the soil column. The tendency for PEST to estimate slightly higher sand content than observed may be due to the unique composition of soils in the WGEW. There is an unusually high rock content in these soils that cannot be accounted for in the Noah model, for which PEST compensates by suggesting higher sand content and, therefore, higher hydraulic conductivity and lower porosity. Both of these results are consistent with high rock content in the soil column.

[52] As indicated in Figure 7 and Table A1, at some locations there seems to be a strong correlation between the density and sampling frequency of precipitation gauges and the estimated soil textures using the PEST-PTF approach. For example, sites 2, 4, 5, and 6 demonstrate a significant decrease in estimated sand content, and an increase in estimated silt content, with decreasing representativeness of the precipitation input data. Such impacts are evident even in the change from use of a collocated precipitation gauge to the use of center-gauge precipitation estimates. For other locations, such as sites 7 and 8, the sand percentages are so high as to be physically meaningless, suggesting that other model formulation or parameter errors may need to be

Table 5. Mean Bias of the Top 5-cm Volumetric Soil Moisture Between the PEST-PTF Method and the PBMR Observations, Averaged Over the Six PBMR Times at All Eight Metflux Sites, for the Simulations With Varied Precipitation Forcing and With FXEXP Also Estimated by PEST[a]

Precipitation	Site 1	Site 2	Site 3	Site 4	Site 5	Site 6	Site 7	Site 8
Interpolated	−0.204	−0.336	−0.070	−0.139	−0.126	−0.215	0.216	0.029
WGEW MAP	−0.151	−0.181	−0.041	0.009	−0.062	−0.071	0.161	0.054
Gauge 33	−0.170	−0.256	−0.088	−0.033	−0.088	−0.134	0.167	0.042

[a]Volumetric soil moisture is given as percent.

corrected in order to produce reasonable, physically meaningful estimates. At two intermediate locations, sites 1 and 3, the estimated sand content actually decreases slightly with less accurate precipitation input, though overall the estimated sand content remains high and silt content remains low at these locations.

[53] The USDA soil texture triangle, along with the results of the precipitation experiments for site 5, is shown in Figure 8. The observed soil class at this site was either sandy loam or sandy clay loam, depending on the source of the classification. A box around each of the observed values indicates the overall range of these observations, given an expected level of representation uncertainty. We must conclude that errors in model formulation, combined with the difficulty of complete optimization using a simple two-parameter PTF as that by *Cosby et al.* [1984], lead to the unlikely estimates of soil content and classification by the PEST-PTF method that are shown in Figure 8.

[54] As noted above, optimized estimates of sand, clay and silt content at several of the simulation sites seem particularly sensitive to the precipitation inputs. To further explore this sensitivity, we examined the change in optimized sand content with respect to several characteristics of the input precipitation, including overall total, average intensity, and frequency of occurrence. The only significant relationship that we have found is shown in Figure 9, which illustrates changes in the estimated sand content with respect to a change in the number of precipitation events detected, based on collocation of the precipitation gauge and soil moisture measurements.

[55] Consistent with the discussion above, there is a decrease in the estimated sand content when the events actually observed at the site are not represented in the input. For example, using the center gauge rather than the precipitation gauge at the site may lead to representation errors as well as those due to spatial variations in the precipitation intensity. Such errors are represented by sites 2, 4, 5, and 6 in the lower left quadrant of Figure 9. This makes conceptual sense, as missed events would lead to a dry bias in simulated soil moisture. To compensate for this dry bias, and according to the PTF shown in equation (3), the PEST-PTF approach will yield a smaller sand content in order to decrease the saturated hydraulic conductivity, which will then decrease the drainage and retain more moisture in the 5-cm surface soil layer.

[56] Conversely, we also find that there is a slight decrease in the estimated sand content when the number of events simulated at the site is greater than that actually observed, owing to the fact that all events in the WGEW are captured when using the full network for calculation of the MAP. These results tend to produce more frequent, lower intensity events than may have been recorded at an individual site, such that the general decrease in event intensity leads to a decrease in the estimated sand content, while the general increase in event frequency increase leads to an increase in the estimated sand content. The net result of these overlapping factors, which are diminished event intensity but at a greater frequency of occurrence, is a slight decrease in the estimated sand content for a given site. We conclude that the ability to detect the occurrence of individual rainfall events at a given location is a key factor in the estimation of soil texture using multitemporal remote sensing and the parameter optimization methods described here.

4.3. Evaporation Parameter Uncertainty

[57] To this point, all of the PEST-derived parameter estimates have been only for soil hydraulic properties, with the PTF constraint also providing soil texture as a byproduct. As in work by *Santanello et al.* [2007], we have not attempted simultaneous calibration of any other parameters in the Noah LSM. However, as shown in Figure 6 and discussed above, a systematic bias was evident in the dry-down period prior to DOY 221 that caused the soil moisture errors on that date to be lower with more distant sources of precipitation forcing. Several Noah model parameters were tested as potential sources of this counterintuitive result. It was found that PEST tended to increase such parameters as the greenness and leaf area index beyond reasonable values in this area in an attempt to increase the rate of evaporation and thus decrease the moisture content of the surface soil layer. Other parameters tested included the minimum stomatal resistance, the water infiltration/runoff parameter, and the bare soil evaporation parameter. The latter was the only parameter for which optimization led to a significant improvement in the results. The final experiments in this work thus combine the estimation of soil hydraulic parameters, under the influence of various input precipitation time series, with estimation of the bare soil evaporation parameter FXEXP in the Noah LSM.

[58] Bare soil evaporation in Noah is derived by multiplying a factor (FX) by the calculated potential evaporation for the fraction of bare soil at each simulation point. The parameter FXEXP determines this factor:

$$\mathrm{FX} = \left(\frac{\mathrm{SMC} - \mathrm{SMCDRY}}{\mathrm{SMCMAX} - \mathrm{SMCDRY}} \right)^{\mathrm{FXEXP}}, \qquad (5)$$

Table 6. Mean RMSE of the Top 5-cm Volumetric Soil Moisture Between the PEST-PTF Method and the PBMR Observations, Averaged Over the Six PBMR Times at All Eight Metflux Sites, for the Simulations With Varied Precipitation Forcing and With FXEXP Also Estimated by PEST[a]

Precipitation	Site 1	Site 2	Site 3	Site 4	Site 5	Site 6	Site 7	Site 8
Interpolated	1.420	1.168	1.726	0.611	0.499	1.012	1.511	1.295
WGEW MAP	2.315	1.060	1.390	0.813	1.186	1.114	1.203	1.458
Gauge 33	1.913	1.092	1.384	1.159	1.511	1.478	1.176	1.045

[a]Volumetric soil moisture is given as percent.

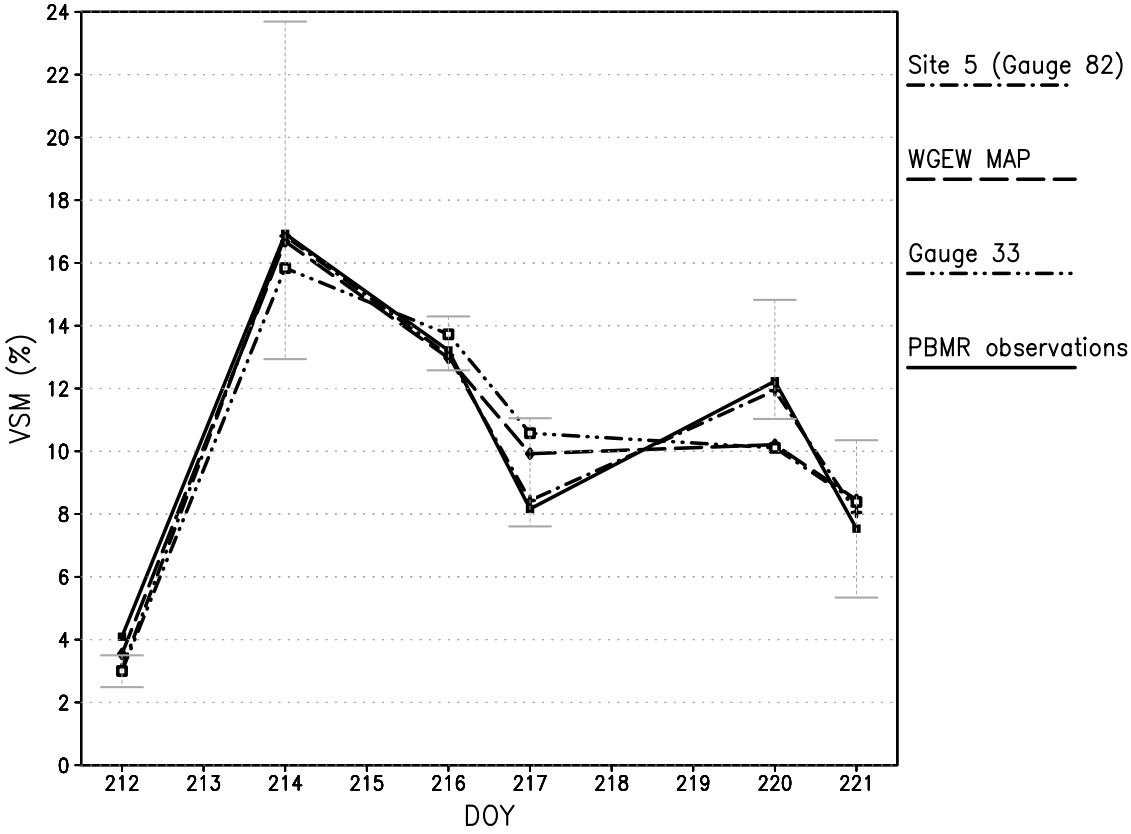

Figure 10. Same as Figure 6, but for the simulations with PEST also estimating the Noah bare soil evaporation parameter FXEXP.

where SMC (m^3 m^{-3}) is the top layer volumetric soil moisture content calculated by the LSM at each time step, SMCDRY is the dry volumetric soil moisture threshold at which direct evaporation from the surface soil layer is halted (SMCDRY = 0.02 m^3 m^{-3} in this work, but is set equal to the vegetation wilting point in a more recent version of the Noah LSM), and SMCMAX is the porosity (m^3 m^{-3}) that is given by equation (1) above. On the basis of the work of *Chen et al.* [1996], FXEXP = 2 is typically selected in order to provide a nonlinear evaporation stress function; however the original Noah LSM value of FXEXP = 1 was found to reproduce better the observed evaporation in WGEW (not shown). Therefore, FXEXP had been set to 1 in the experiments described above, as in work by *Santanello et al.* [2007].

[59] Tables 5 and 6 list the estimated surface-layer soil moisture bias and RMSE, respectively, at the eight Metflux sites in the WGEW for PEST-PTF experiments, similar to those shown in Tables 3 and 4, except that here PEST has been allowed to adjust the FXEXP parameter in the Noah LSM as well. The RMSE in Table 6 is improved, in comparison with that shown in Table 4, for all sites and input precipitation variations. These results demonstrate that optimization of key parameters in the LSM to allow both drainage and evaporation from the surface soil layer, in order to best fit the given observations, results in the best possible simulation under a given input precipitation time series. For experiments that employ precipitation gauges collocated with the soil moisture observations, the RMSE is reduced on average from about 1.5%, for the optimization that ignores FXEXP, to about 1.2%. Although this difference is rather small, at site 7 the difference is more significant, with an RMSE reduction from about 2.5% to 1.5%. As above, optimization experiments using the Tucson gauge and NARR forcing did not converge on a solution, which again underscores the importance of input precipitation sources that are able to detect the observed rainfall events in the watershed and nearest the point of interest.

[60] In comparing Tables 3 and 5, we find that biases are reduced when using the collocated precipitation gauges or interpolated values for sites 3, 7, and 8, which are three of the sites with the largest estimated sand content as shown in Figure 7. The estimated sand content values at these sites were also least sensitive to the number of events, as shown in Figure 9. The additional optimization of FXEXP at these sites resulted in estimated soil textures that are more consistent with those at the other locations, as discussed below.

[61] The biases in Table 5 are most improved in those simulations that employed the mean or center-gauge precipitation forcing. This improvement suggests that, in the absence of the best available precipitation forcing, allowing the LSM additional freedom in the optimization process can result in lower soil moisture biases. When using the best available precipitation forcing, and at locations other than sites 3, 7, and 8 as noted above, this freedom does not result in much additional bias improvement, given the limited number of soil moisture observations and the forcing used

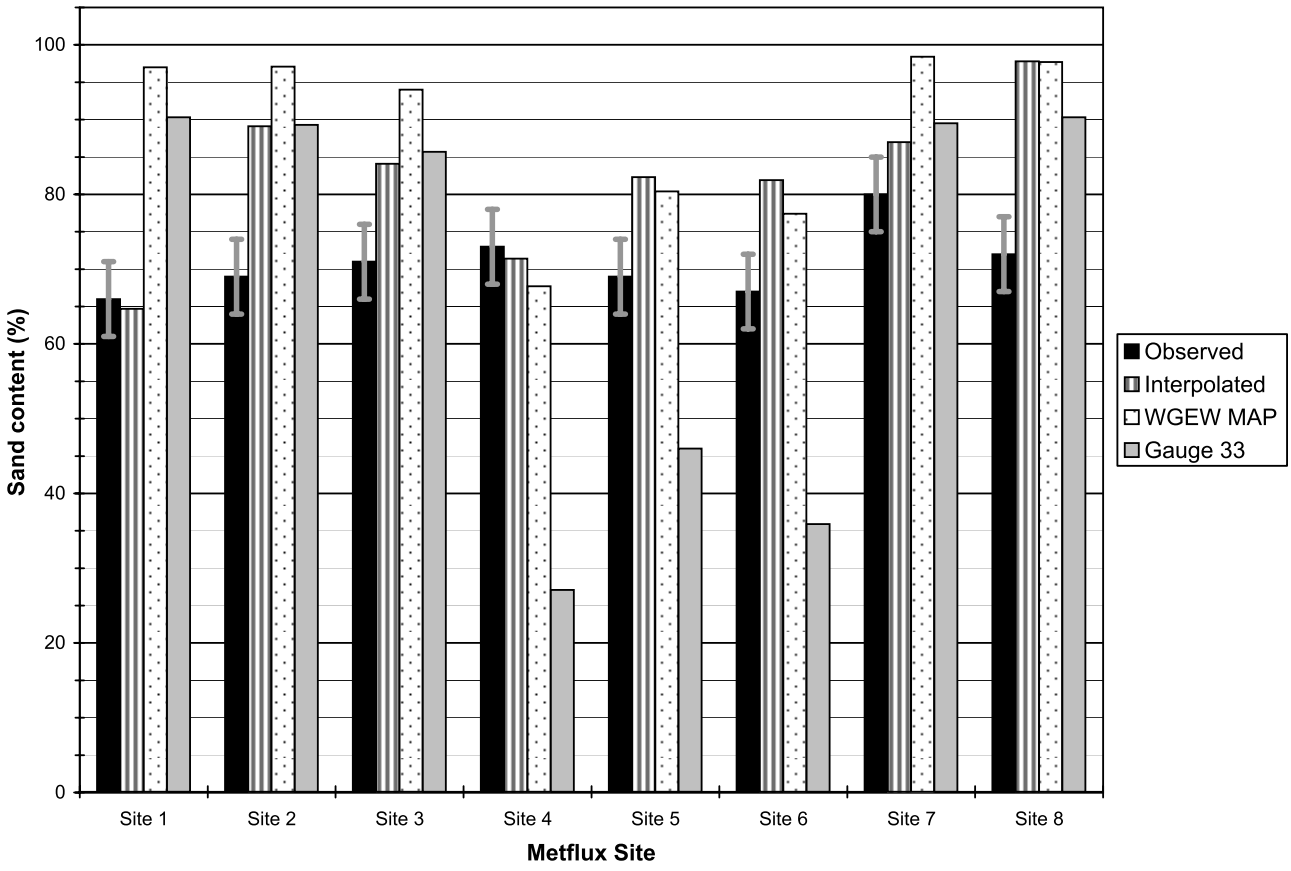

Figure 11. Same as Figure 7, but for the simulations with PEST also estimating the Noah bare soil evaporation parameter FXEXP.

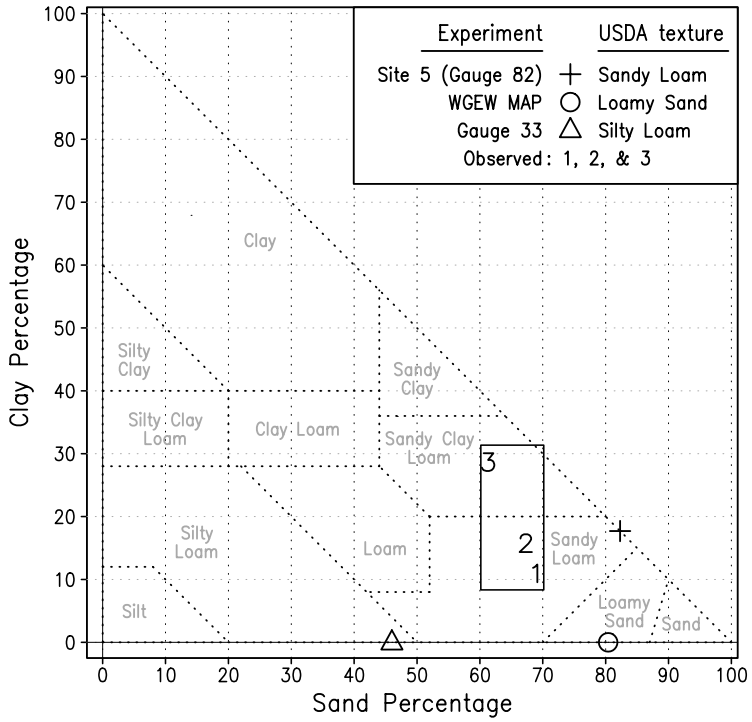

Figure 12. Same as Figure 8, but for the simulations with PEST also estimating the Noah bare soil evaporation parameter FXEXP.

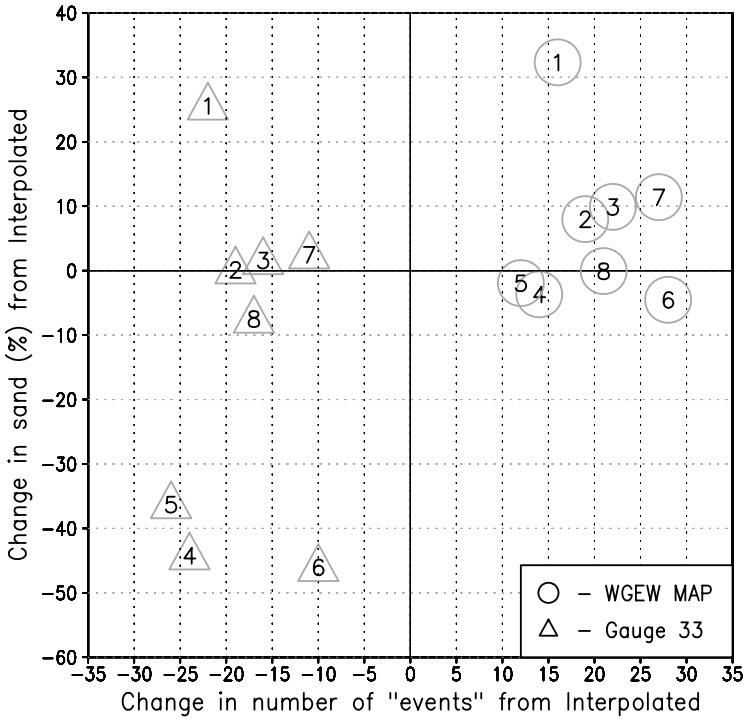

Figure 13. Same as Figure 9, but for the simulations with PEST also estimating the Noah bare soil evaporation parameter FXEXP.

in these experiments. Clearly, to fully explore the tradeoffs between observation frequency and precipitation accuracy for soil hydrologic parameter estimation, a future soil moisture campaign or mission with more observations over a longer period would be required.

[62] The simulated soil moisture content for these experiments at site 5, with error bars based on in situ measurements, and calculated biases in relation to PBMR observations, are shown in Figure 10. These results may be compared with those given in Figure 6 for the experiments in which FXEXP was held fixed. These results demonstrate that the bias is improved at all PBMR observation times, most notably at two times: early in the simulation period before the intense precipitation event on 1 August 1990 (DOY 213), and through the drying period up to 9 August (DOY 221). It is during these relatively dry periods that the bare soil evaporation, together with the high sand content, produces the best possible soil moisture simulations.

[63] The sand content at each location that was estimated in the experiments for which PEST was also allowed to adjust FXEXP are shown in Figure 11, and the full sand-silt-clay estimates are given in Appendix A (Table A2). The simulations using the best available precipitation lead to lower estimates of sand content than shown in Figure 7, and are generally much closer to the observed sand content observed at the respective sites. As expected, removal of the model formulation error allows the optimization system to produce not only more accurate soil moisture estimates, but also more reasonable estimates of soil texture. The optimization of FXEXP values allows the LSM to remove additional soil moisture from the topsoil layer by evaporation, rather than by increasing the estimated sand content in order to increase the soil drainage capacity. Figure 11 demonstrates that the results remain sensitive to the accuracy of the precipitation input, but also confirms the expected result, that use of the full WGEW precipitation gauge network as shown in Figure 2 produces estimates of soil texture that are closest to the observed texture.

[64] A graphical representation of results for site 5 on the USDA soil texture triangle is shown in Figure 12. In this case, the experiment using collocated precipitation gauge data correctly estimates a sandy loam soil texture, with a reasonable estimate of clay percentage compared to the noninterpolated results, although the estimated sand percentage is high. Generally, as shown in Table A2, the additional calibration of the FXEXP parameter leads to PEST-estimated soil textures that are closer to those observed at all Metflux sites in the WGEW than obtained in experiments for which FXEXP was held constant. It is also found that the experiments using center-gauge precipitation, which had previously resulted in small estimates of sand content, tended with flexibility in the value of FXEXP to result in higher estimates of sand content, and thus overall soil textures closer to those observed. We find that there is less variation in the estimated values of sand content with changes in the input precipitation source than in previous experiments, as shown in Figure 12.

Table 7. Estimated FXEXP Values at All Eight Metflux Sites for the PEST-PTF Simulations With Varied Precipitation Forcing

Precipitation	Site 1	Site 2	Site 3	Site 4	Site 5	Site 6	Site 7	Site 8
Interpolated	0.779	1.026	0.824	0.897	0.765	0.805	0.614	0.818
WGEW MAP	0.866	1.133	0.893	1.157	1.260	1.062	0.576	0.791
Gauge 33	0.920	1.119	0.907	1.041	1.162	0.956	0.614	0.830

[65] Figure 13, like Figure 8, shows the response of the optimization system in the estimation of both sand content and FXEXP to changes in the number of precipitation events. As noted above, sites 3, 7, and 8 are those with the highest estimated sand content (see Figure 7) and are the least sensitive to the number of precipitation events (see Figure 9). The results in Figure 13 suggest that the optimization of FXEXP at these locations lends to a greater commonality with the other sites in the soil hydraulic response to wetting and drying periods. Further comparisons of Figures 9 and 13 suggest that the PEST-PTF approach in which adjustment of FXEXP is allowed produces a more intuitive and physically consistent response of the estimated sand content to the number of detected precipitation events. As before, precipitation input that included a lower number of detected events was found to result in soil textures with lower estimated sand content, while precipitation input with a number of detected events closer to that actually observed at individual locations with collocated gauges were found to result in soil textures with greater estimated sand content.

[66] Values of FXEXP resulting from these latter simulations are listed in Table 7. The values fall, for the most part, around the default value of FXEXP = 1 as employed previously, depending on location. Sites that previously demonstrated high values of estimated sand content, in experiments with FXEXP held fixed, are found to have optimal FXEXP values less than unity, which result in greater evaporation from bare soil areas during the simulation period. In particular, sites 7 and 8 had previously estimated sand content values near 100%, but with allowances for variation in FXEXP have estimated values for that parameter among the lowest of all the study sites. As shown in Figure 11, estimation of FXEXP along with the soil texture results in smaller RMS errors in surface soil moisture at the individual PBMR observation times, indicating the interaction between bare soil evaporation (via FXEXP) and soil drainage (via sand content) in the reduction of simulation biases. Although the estimation of FXEXP reduced the simulation error for soil moisture, remaining errors can likely be attributed to other inconsistencies and deficiencies in the model formulation.

Table A1. PEST-Estimated Soil Properties Using the *Cosby et al.* [1984] PTF at All Eight Metflux Sites for the Simulations With Varied Precipitation Forcing[a]

Site	Precipitation Source	SAND (%)	CLAY (%)	SILT (%)
1	Interpolated	95.3	4.7	0.0
1	WGEW MAP	77.0	0.0	23.0
1	Gauge 33	92.2	7.8	0.0
1	**Observed**	**66.0 ± 5**	**10.0 ± 5**	**24.0 ± 5**
2	Interpolated	88.5	11.5	0.0
2	WGEW MAP	75.7	0.0	24.3
2	Gauge 33	47.9	0.0	52.1
2	**Observed**	**69.0 ± 5**	**11.0 ± 5**	**20.0 ± 5**
3	Interpolated	90.9	9.1	0.0
3	WGEW MAP	95.8	4.2	0.0
3	Gauge 33	88.0	12.0	0.0
3	**Observed**	**71.0 ± 5**	**9.0 ± 5**	**20.0 ± 5**
4	Interpolated	85.5	14.5	0.0
4	WGEW MAP	58.5	0.0	41.5
4	Gauge 33	23.7	0.0	76.3
4	**Observed**	**73.0 ± 5**	**5.0 ± 5**	**22.0 ± 5**
5	Interpolated	88.3	11.7	0.0
5	WGEW MAP	64.8	0.0	35.2
5	Gauge 33	31.7	0.0	68.3
5	**Observed**	**69.0 ± 5**	**11.0 ± 5**	**20.0 ± 5**
6	Interpolated	89.1	10.9	0.0
6	WGEW MAP	73.7	0.0	26.3
6	Gauge 33	42.0	0.0	58.0
6	**Observed**	**67.0 ± 5**	**8.0 ± 5**	**25.0 ± 5**
7	Interpolated	98.3	1.7	0.0
7	WGEW MAP	100.0	0.0	0.0
7	Gauge 33	99.4	0.6	0.0
7	**Observed**	**80.0 ± 5**	**6.0 ± 5**	**14.0 ± 5**
8	Interpolated	100.0	0.0	0.0
8	WGEW MAP	100.0	0.0	0.0
8	Gauge 33	94.4	5.6	0.0
8	**Observed**	**72.0 ± 5**	**8.0 ± 5**	**20.0 ± 5**

[a]"Observed" values are those provided by *Schmugge et al.* [1994].

Table A2. As in Table A1, but With FXEXP Also Estimated by PEST

Site	Precipitation Source	SAND (%)	CLAY (%)	SILT (%)
1	Interpolated	64.7	0.0	35.3
1	WGEW MAP	97.0	3.0	0.0
1	Gauge 33	90.3	9.7	0.0
1	**Observed**	**66.0 ± 5**	**10.0 ± 5**	**24.0 ± 5**
2	Interpolated	89.1	10.9	0.0
2	WGEW MAP	97.1	2.9	0.0
2	Gauge 33	89.3	10.7	0.0
2	**Observed**	**69.0 ± 5**	**11.0 ± 5**	**20.0 ± 5**
3	Interpolated	84.1	15.9	0.0
3	WGEW MAP	94.0	6.0	0.0
3	Gauge 33	85.7	14.3	0.0
3	**Observed**	**71.0 ± 5**	**9.0 ± 5**	**20.0 ± 5**
4	Interpolated	71.4	12.6	16.1
4	WGEW MAP	67.7	0.0	32.3
4	Gauge 33	27.1	0.0	72.9
4	**Observed**	**73.0 ± 5**	**5.0 ± 5**	**22.0 ± 5**
5	Interpolated	82.3	17.7	0.0
5	WGEW MAP	80.4	0.0	19.6
5	Gauge 33	46.0	0.0	54.0
5	**Observed**	**69.0 ± 5**	**11.0 ± 5**	**20.0 ± 5**
6	Interpolated	81.9	18.1	0.0
6	WGEW MAP	77.4	0.0	22.6
6	Gauge 33	35.9	0.0	64.1
6	**Observed**	**67.0 ± 5**	**8.0 ± 5**	**25.0 ± 5**
7	Interpolated	87.0	13.0	0.0
7	WGEW MAP	98.4	1.6	0.0
7	Gauge 33	89.5	10.5	0.0
7	**Observed**	**80.0 ± 5**	**6.0 ± 5**	**14.0 ± 5**
8	Interpolated	97.8	2.2	0.0
8	WGEW MAP	97.7	2.3	0.0
8	Gauge 33	90.3	9.7	0.0
8	**Observed**	**72.0 ± 5**	**8.0 ± 5**	**20.0 ± 5**

5. Summary and Conclusions

[67] This work extends the recent study by *Santanello et al.* [2007] in which it was shown that soil texture and associated hydraulic parameters may be estimated using a combination of multitemporal microwave remote sensing, land surface modeling, and parameter estimation methods. As in that study, the LIS modeling framework was employed with the Noah LSM, additional specification of PTFs after *Cosby et al.* [1984], and parameter optimization using PEST. Using selected sites in the WGEW that were instrumented and observed during the M90 experiment, this system was applied as part of ongoing development of the

Army Remote Moisture System (ARMS) [*Tischler et al.*, 2006].

[68] This approach was demonstrated and results were obtained for the optimized soil textures using varied initial soils data at each of the eight M90 Metflux sites in the WGEW, and it was shown that the system could produce simulated surface soil moisture values with RMS errors of about 1.5% or less, compared with about 4% RMSE when standard soil classes from FAO, STATSGO or SSURGO data sets and the default hydraulic parameter tables in the Noah LSM were employed. The precipitation time series at each site was then systematically varied using available observations and estimates, including those from the synoptic precipitation gauge closest to WGEW (Tucson, Arizona) and analyzed results from the NARR data set. A significant finding of this work was that our approach to the estimation of soil textures did not result in a convergent solution when using the Tucson precipitation gauge or NARR estimate to provide input precipitation, highlighting the importance of using in situ precipitation gauges for appropriate representation of the primary forcing variables. In addition, it was found that the accuracy of soil texture estimates remained sensitive to the number of events represented in the input precipitation time series compared to those that were observed at gauge locations within the WGEW, with fewer simulated events than observed leading to the estimation of less sandy soils and estimated soil textures farther from those observed at the WGEW Metflux sites.

[69] The importance of calibrated hydraulic parameters for the accurate simulation of soil moisture infiltration, and their interaction with the evaporation of surface moisture from bare soils in the semiarid environment of the WGEW, in the estimation of reasonable effective soil textures was demonstrated by repetition of the precipitation sensitivity study with simultaneous optimization of the bare soil evaporation parameter FXEXP in the Noah LSM. This multiparameter calibration resulted in the lowest volumetric soil moisture RMS errors in this study, reducing errors in volumetric soil moisture content across the eight Metflux sites in the WGEW to about 1.2%.

[70] In addition to the improvement in simulated surface soil moisture content, the multiparameter calibration approach generally resulted in improved estimates of soil texture as well as a more consistent response of the estimated sand content to the number of simulated precipitation events, relative to those observed at each site. After optimization of the FXEXP parameter, the estimated sand content at each site was more accurate when also using the observed or interpolated precipitation from the full WGEW gauge network, in contrast with the results before optimization of the FXEXP parameter which demonstrated uniformly high estimates of sand content. As above, the simulation of fewer precipitation events than observed at the Metflux sites was found to result in estimates of less sandy soils than measured. However, comparison of the simulation sensitivity to the number of precipitation events both before and after optimization of the FXEXP parameter suggests that a more consistent simulation response is obtained by allowing for increased evaporation from bare soils than initially indicated in the Noah LSM, thereby reducing the dependence on infiltration, and thus the adjustment of hydraulic parameters to unphysical values, to compensate for wet biases in the simulated surface soil moisture results.

[71] There are many caveats to this study, including the limited time period, single LSM, simple calibration approach, single PTF, and limited validation data. However, this study is an important step toward the estimation of soil texture and hydraulic properties using multitemporal remote sensing data. This study is limited geographically to the WGEW and to the aircraft-based PBMR observations obtained during the M90 experiment. Recent results for the retrieval of surface soil moisture from satellites (e.g., RADARSAT) by the Delta Index approach, described by *Thoma et al.* [2006] and demonstrated for use in parameter estimation approaches by *Santanello et al.* [2007], provide a pathway toward the operational estimation of both surface soil moisture values and soil textures. These methods will be further tested in simulations for locations with precipitation climatologies and soil textures significantly different from those found at the WGEW, such as Little River, Georgia; Little Washita, Oklahoma; and North Park, Colorado. Further refinement of the methods in this, and previous, studies will help pave the way for applications of future remote sensing missions oriented on soil moisture observations, such as the upcoming NASA SMAP mission.

Appendix A

[72] The appendix gives the observed and estimated sand, silt, and clay percentages at each Metflux site using three different precipitation sources. The estimates in Table A1 are obtained using the PTF-constrained LIS-PEST with a fixed value of FXEXP, while the estimates in Table A2 show the PTF-constrained LIS-PEST results with a simultaneous estimation of FXEXP.

[73] **Acknowledgments.** The authors appreciate the support of the USACE-ERDC-TEC and the USDA-ARS-SWRC. This work was performed under USDA-ARS reimbursable agreement 60-5342-3-0363 and was conducted primarily at NASA-GSFC. Special thanks are extended to T. Schmugge for insight into the PBMR retrieval process, P. R. Houser for the use of collected WGEW input fields and data sets, J. Doherty for help in understanding the PEST formulation and procedure, S. V. Kumar for help with the integration of PEST in LIS, and to the office and field crews at the WGEW for their untiring efforts.

References

Albertson, J. D., and N. Montaldo (2003), Temporal dynamics of soil moisture variability: 1. Theoretical basis, *Water Resour. Res.*, *39*(10), 1274, doi:10.1029/2002WR001616.

Berbery, E. H., Y. Luo, K. E. Mitchell, and A. K. Betts (2003), Eta model estimated land surface processes and the hydrologic cycle of the Mississippi basin, *J. Geophys. Res.*, *108*(D22), 8852, doi:10.1029/2002JD003192.

Betts, A. K. (2000), Idealized model for equilibrium boundary layer over land, *J. Hydrometeorol.*, *1*, 507–523.

Betts, A. K., J. H. Ball, M. Bosilovich, P. Viterbo, Y.-C. Zhang, and W. B. Rossow (2003), Intercomparison of water and energy budgets for five Mississippi subbasins between ECMWF reanalysis (ERA-40) and NASA Data Assimilation Office fvGCM for 1990–1999, *J. Geophys. Res.*, *108*(D16), 8618, doi:10.1029/2002JD003127.

Bowling, L. C., et al. (2003), Simulation of high-latitude hydrological processes in the Torne-Kalix basin: PILPS phase 2(e). Parts 1 and 2, *Global Planet. Change*, *38*(1–2), 1–30.

Braun, F. J., and G. Schadler (2005), Comparison of soil hydraulic parameterizations for mesoscale meteorological models, *J. Appl. Meteorol.*, *44*(7), 1116–1132.

Brooks, R. H., and A. T. Corey (1964), Hydraulic properties of porous media, *Hydrol. Pap. 3*, 24 pp., Colo. State Univ., Fort Collins.

Campbell, G. S. (1974), A simple method for determining unsaturated conductivity from moisture retention data, *Soil Sci.*, *117*(6), 311–314.

Carlson, T. N., R. R. Gillies, and T. J. Schmugge (1995), An interpretation of methodologies for indirect measurement of soil water content, *Agric. For. Meteorol.*, *77*(3–4), 191–205.

Chen, F., K. Mitchell, J. Schaake, Y.-K. Xue, H.-L. Pan, V. Koren, Q.-Y. Duan, M. Ek, and A. Betts (1996), Modeling of land surface evaporation by four schemes and comparison with FIFE observations, *J. Geophys. Res.*, *101*(D3), 7251–7268.

Clapp, R. B., and G. M. Hornberger (1978), Empirical equations for some soil hydraulic properties, *Water Resour. Res.*, *14*(4), 601–604.

Cornelis, W. M., J. Ronsyn, M. Van Meirvenne, and R. Hartmann (2001), Evaluation of pedotransfer functions for predicting the soil moisture retention curve, *Soil Sci. Soc. Am. J.*, *65*, 638–648.

Cosby, B. J., G. M. Hornberger, R. B. Clapp, and T. R. Ginn (1984), A statistical exploration of the relationships of soil moisture characteristics to the physical properties of soils, *Water Resour. Res.*, *20*(6), 682–690.

Cuenca, R. H., M. Ek, and L. Mahrt (1996), Impact of soil water property parameterization on atmospheric boundary layer simulation, *J. Geophys. Res.*, *101*(D3), 7269–7277.

Doherty, J. (2004), *Model-Independent Parameter Estimation: User Manual*, 5th ed., Watermark Numer. Comput., Brisbane, Queensl., Australia.

Ek, M. B., and A. A. M. Holtslag (2004), Influence of soil moisture on boundary layer cloud development, *J. Hydrometeorol.*, *5*, 86–99.

Ek, M. B., K. E. Mitchell, Y. Lin, E. Rogers, P. Grunmann, V. Koren, G. Gayno, and J. D. Tarpley (2003), Implementation of Noah land surface model advances in the National Centers for Environmental Prediction operational mesoscale Eta model, *J. Geophys. Res.*, *108*(D22), 8851, doi:10.1029/2002JD003296.

Entekhabi, D., H. Nakamura, and E. G. Njoku (1994), Solving the inverse problems for soil moisture and temperature profiles by sequential assimilation of multifrequency remotely-sensed observations, *IEEE Trans. Geosci. Remote Sens.*, *32*(2), 438–448.

Feddes, R. A., M. Menenti, P. Kabat, and W. G. M. Bastiaanssen (2003), Is large-scale inverse modeling of unsaturated flow with areal average evaporation and surface soil moisture as estimated from remote-sensing feasible?, *J. Hydrol.*, *143*(1–2), 125–152.

Findell, K. L., and E. A. B. Eltahir (2003), Atmospheric controls on soil moisture-boundary layer interactions. Part I: Framework development, *J. Hydrometeorol.*, *4*, 552–569.

Food and Agriculture Organization (1996), *Digitized Soil Map of the World, Including Derived Soil Properties* [CD-ROM], Rome.

Garcia, M., C. D. Peters-Lidard, and D. Goodrich (2008), Spatial interpolation of precipitation in a dense gauge network for monsoon storm events in the southwestern U.S., *Water Resour. Res.*, *44*, W05S13, doi:10.1029/2006WR005788.

Gupta, H. V., L. A. Bastidas, S. Sorooshian, W. J. Shuttleworth, and Z. L. Yang (1999), Parameter estimation of a land-surface scheme using multicriteria methods, *J. Geophys. Res.*, *104*(D16), 19,491–19,503.

Gutmann, E. D., and E. E. Small (2005), The effect of soil hydraulic properties vs. soil texture in land surface models, *Geophys. Res. Lett.*, *32*, L02402, doi:10.1029/2004GL021843.

Hess, R. (2001), Assimilation of screen level observations by variational soil moisture analysis, *Meteorol. Atmos. Phys.*, *77*(1–4), 145–154.

Higgins, W., et al. (2006), The NAME 2004 field campaign and modeling strategy, *Bull. Am. Meteorol. Soc.*, *87*, 79–94.

Hogue, T. S., L. Bastidas, H. Gupta, S. Sorooshian, K. Mitchell, and W. Emmerich (2005), Evaluation and transferability of the Noah land surface model in semiarid environments, *J. Hydrometeorol.*, *6*, 68–84.

Hollenbeck, K. J., T. J. Schmugge, G. M. Hornberger, and J. R. Wang (1996), Identifying soil hydraulic heterogeneity by detection of relative change in passive microwave remote sensing observations, *Water Resour. Res.*, *32*(1), 139–148.

Hollinger, S. E., and S. A. Isard (1994), A soil moisture climatology of Illinois, *J. Clim.*, *7*(5), 822–833.

Houser, P. R. (1996), Remote sensing soil moisture using four-dimensional data assimilation, Ph.D. dissertation, Dep. of Hydrol. and Water Resour., Univ. of Ariz., Tucson.

Houser, P. R., W. J. Shuttleworth, J. S. Famiglietti, H. V. Gupta, K. H. Syed, and D. C. Goodrich (1998), Integration of soil moisture remote sensing and hydrologic modeling using data assimilation, *Water Resour. Res.*, *34*(12), 3405–3420.

Hymer, D. C., M. S. Moran, and T. O. Keefer (2000), Soil water evaluation using a hydrological model and calibrated sensor network, *Soil Sci. Soc. Am. J.*, *64*, 319–326.

Koster, R. D., et al. (2004), Regions of strong coupling between soil moisture and precipitation, *Science*, *305*(5687), 1138–1140.

Kumar, S. V., et al. (2006), Land Information System—An interoperable framework for high resolution land surface modeling, *Environ. Model. Software*, *21*(10), 1402–1415.

Kustas, W. P., and D. C. Goodrich (1994), Monsoon '90 multidisciplinary experiment, *Water Resour. Res.*, *30*(5), 1211–1225.

Liu, Y., L. A. Bastidas, H. V. Gupta, and S. Sorooshian (2003), Impacts of a parameterization deficiency on offline and coupled land surface model simulations, *J. Hydrometeorol.*, *4*, 901–914.

Liu, Y., H. V. Gupta, S. Sorooshian, L. A. Bastidas, and W. J. Shuttleworth (2004), Exploring parameter sensitivities of the land surface using a locally coupled land-atmosphere model, *J. Geophys. Res.*, *109*, D21101, doi:10.1029/2004JD004730.

Liu, Y., H. V. Gupta, S. Sorooshian, L. A. Bastidas, and W. J. Shuttleworth (2005), Constraining land surface and atmospheric parameters of a locally coupled model using observational data, *J. Hydrometeorol.*, *6*, 156–172.

Lunetta, R. S., and J. A. Sturdevant (1993), The North American Landscape Characterization Landsat Pathfinder Project, in *Pecora 12 Symposium, Land Information from Space-Based Systems, Proceedings*, edited by L. R. Pettinger, pp. 363–371, Am. Soc. of Photogramm. and Remote Sens., Bethesda, Md.

Mesinger, F., et al. (2006), North American regional reanalysis, *Bull. Am. Meteorol. Soc.*, *87*(3), 343–360.

Miller, D. A., and R. A. White (1998), A conterminous United States multilayer soil characteristics dataset for regional climate and hydrology modeling, *Earth Interact.*, *2*(2–002), 26 pp.

Miller, D. A., G. W. Peterson, and M. N. Lakhtakia (1994), Using the State Soil Geographic Database (STATSGO) for regional atmospheric modeling, paper presented at Annual Meeting, Soil Sci. Soc. of Am., Seattle, Wash.

Mohanty, B. P., P. J. Shouse, D. A. Miller, and M. T. van Genuchten (2002), Soil property database: Southern Great Plains 1997 Hydrology Experiment, *Water Resour. Res.*, *38*(5), 1047, doi:10.1029/2000WR000076.

Moran, M. S., C. D. Peters-Lidard, J. M. Watts, and S. McElroy (2004), Estimating soil moisture at the watershed scale with satellite-based radar and land surface models, *Can. J. Remote Sens.*, *30*(5), 805–826.

Nachtergaele, F. O. (2003), From the soil map of the world to the digital global soil and terrain database: 1960–2002, report, Soil Resour., Land and Water Dev. Div., U.N. Food and Agric. Org., Rome.

Pitman, A. J. (2003), The evolution of, and revolution in, land surface schemes designed for climate models, *Int. J. Climatol.*, *23*(5), 479–510, doi:10.1002/joc.893.

Rawls, W. J., D. L. Brakensiek, and K. E. Saxton (1982), Estimation of soil water properties, *Trans. Am. Soc. Agric. Eng.*, *25*(5), 1316–1320.

Reynolds, C. A., T. J. Jackson, and W. J. Rawls (1999), Estimating available water content by linking the FAO Soil Map of the World with global soil profile databases and pedo-transfer functions, *Eos Trans. AGU*, *80*(17), Spring Meet. Suppl., H41D-12.

Richards, L. A. (1931), Capillary conduction of liquids through porous mediums, *J. Appl. Phys.*, *1*, 318–333.

Robock, A., K. Y. Vinnikov, G. Srinivasan, J. K. Entin, S. E. Hollinger, N. A. Speranskaya, S. Liu, and A. Namkhai (2000), The Global Soil Moisture Data Bank, *Bull. Am. Meteorol. Soc.*, *81*(6), 1281–1299.

Santanello, J. A., Jr., and T. N. Carlson (2001), Mesoscale simulation of rapid soil drying and its implications for predicting daytime temperature, *J. Hydrometeorol.*, *2*, 71–88.

Santanello, J. A., Jr., C. D. Peters-Lidard, M. Garcia, D. M. Mocko, M. E. Tischler, M. S. Moran, and D. P. Thoma (2007), Using remotely-sensed estimates of soil moisture to infer soil texture and hydraulic properties across a semi-arid watershed, *Remote Sens. Environ.*, *110*, 79–97, doi:10.1016/j.rse.2007.02.007.

Schaap, M. G., F. J. Leij, and M. T. van Genuchten (1998), Neural network analysis for hierarchical prediction for soil hydraulic properties, *Soil Sci. Soc. Am. J.*, *62*, 847–855.

Schaefer, G. L., and R. F. Paetzold (2001), SNOTEL (SNOwpack TELemetry) and SCAN (Soil Climate Analysis Network), in *Proceedings of an International Workshop on Automated Weather Stations for Applications in Agriculture and Water Resources Management*, *AGM-3 WMO/TD 1074*, World Meteorol. Org., Lincoln, Nebr.

Schlosser, C. A., A. G. Slater, A. Robock, A. J. Pitman, K. Y. Vinnikov, A. Henderson-Sellers, N. A. Speranskaya, and K. Mitchell (2000), Simulations of a boreal grassland hydrology at Valdai, Russia: PILPS phase 2(d), *Mon. Weather Rev.*, *128*(2), 301–321.

Schmugge, T., T. J. Jackson, W. P. Kustas, R. Roberts, R. Parry, D. C. Goodrich, S. A. Amer, and M. A. Weltz (1994), Push Broom Microwave Radiometer observations of surface soil moisture in Monsoon '90, *Water Resour. Res.*, *30*(5), 1321–1327.

Scott, R. L., W. J. Shuttleworth, T. O. Keefer, and A. W. Warrick (2000), Modeling multiyear observations of soil moisture recharge in the semiarid American southwest, *Water Resour. Res.*, *36*(8), 2233–2247.

Shao, Y., and A. Henderson-Sellers (1996), Modeling soil moisture: A project for intercomparison of land surface parameterization schemes Phase 2(b), *J. Geophys. Res.*, *101*(D3), 7227–7250.

Sobieraj, J. A., H. Elsenbeer, and R. A. Vertessy (2001), Pedotransfer functions for estimating saturated hydraulic conductivity: Implications for modeling storm flow generation, *J. Hydrol.*, *251*(3–4), 202–220.

Soet, M., and J. N. M. Stricker (2003), Functional behaviour of pedotransfer functions in soil water flow simulation, *Hydrol. Processes*, *17*(8), 1659–1670.

Thoma, D. P., M. S. Moran, R. Bryant, M. Rahman, C. D. Holifield-Collins, S. Skirvin, E. E. Sano, and K. Slocum (2006), Comparison of four models to determine surface soil moisture from C-band radar imagery in a sparsely vegetated semiarid landscape, *Water Resour. Res.*, *42*, W01418, doi:10.1029/2004WR003905.

Tischler, M., M. Garcia, C. D. Peters-Lidard, M. S. Moran, S. Miller, D. Thoma, S. Kumar, and J. Geiger (2006), A GIS framework for surface-layer soil moisture estimation combining satellite radar measurements and land surface modeling with soil physical property estimation, *Environ. Model. Software*, *22*, 891–898, doi:10.1016/j.envsoft.2006.05.022.

U.S. Department of Agriculture, Natural Resources Conservation Service (2006), Soil Survey Geographic (SSURGO) database for Cochise County, Arizona, Douglas-Tombstone Part, http://soildatamart.nrcs.usda.gov/, Washington, D.C.

M. Garcia, UMBC GEST and Hydrological Sciences Branch, NASA Goddard Space Flight Center, Code 614.3, Greenbelt, MD 20771, USA. (matthew.garcia@nasa.gov)

D. M. Mocko, SAIC and Climate and Radiation Branch, NASA Goddard Space Flight Center, Code 613.2, Greenbelt, MD 20771, USA. (david.mocko@nasa.gov)

M. S. Moran, Southwest Watershed Research Center, USDA Agricultural Research Service, 2000 East Allen Road, Tuscon, AZ 85719, USA. (smoran@tucson.ars.ag.gov)

C. D. Peters-Lidard, Hydrological Sciences Branch, NASA Goddard Space Flight Center, Code 614.3, Greenbelt, MD 20771, USA. (christa.peters@nasa.gov)

J. A. Santanello Jr., UMCP ESSIC and Hydrological Sciences Branch, NASA Goddard Space Flight Center, Code 614.3, Greenbelt, MD 20771, USA. (joseph.santanello@nasa.gov)

M. A. Tischler, Topographic Engineering Center, Engineer Research and Development Center, U.S. Army Corps of Engineers, 7701 Telegraph Road, Alexandria, VA 22315, USA. (michael.a.tischler@erdc.usace.army.mil)

Y. Wu, Science Applications International Corporation, NOAA National Weather Service, National Centers for Environmental Prediction, 5200 Auth Road, Camp Springs, MD 20746-4304, USA. (yihua.wu@noaa.gov)